Spin transport in graphene - hexagonal boron nitride van der Waals heterostructures

Gurram, Mallikarjuna

Chapter 8

Electrical spin injection, transport, and detection in graphene-hexagonal boron nitride van der Waals heterostructures: progress and perspectives

Abstract

The current research in graphene spintronics strives for achieving a long spin lifetime, and efficient spin injection and detection in graphene. In this article, we review how hexagonal boron nitride (hBN) has evolved as a crucial substrate, as an encapsulation layer, and as a tunnel barrier for manipulation and control of spin lifetimes and spin injection/detection polarizations in graphene spin valve devices. First, we give an overview of the challenges due to conventional SiO_2/Si substrate for spin transport in graphene followed by the progress made in hBN based graphene heterostructures. Then we discuss in detail the shortcomings and developments in using conventional oxide tunnel barriers for spin injection into graphene followed by introducing the recent advancements in using the crystalline single/bi/tri-layer hBN tunnel barriers for an improved spin injection and detection which also can facilitate two-terminal spin valve and Hanle measurements at room temperature, and are of technological importance. A special case of bias induced spin polarization of contacts with exfoliated and chemical vapour deposition (CVD) grown hBN tunnel barriers is also discussed. Further, we give our perspectives on utilizing graphene-hBN heterostructures for future developments in graphene spintronics.

8.1 Introduction

Spin injection, transport, and detection are three fundamental processes in spintronics, and the control over these processes is crucial for designing new types of spintronic devices.Various materials have been investigated to realize these phenomena for practical spintronic applications. Graphene has found its place in spintronics due to its favourable properties such as low spin-orbit coupling and small hyperfine interactions [1, 2]. Besides, graphene offers a large carrier mobility and an electrostatic-gate tunable carrier density from the electrons to the holes regime. In the past decade,

This chapter is currently under review as **M. Gurram**, S. Omar, B.J. van Wees, Submitted to *2D Materials*, (2017). ArXiv:1712.07828. (Review article)

a huge amount of research has been carried out in a direction towards bringing graphene's predicted expectations to realize practical applications. Much of the effort has gone into finding solutions to the key challenges in graphene spintronics including, among many others, finding effective tunnel barriers for efficient spin injection and detection, and a clean environment for long distance spin transport in graphene. Along the way, the discovery of various two-dimensional (2D) materials with distinctive physical properties and the possibility of fabricating van der Waals (vdW) heterostructures with graphene, has increased the figure of merit of graphene spintronic devices. Especially, recent findings of using hexagonal boron nitride (hBN) as a substrate and as a tunnel barrier for graphene spin valve devices has attracted a lot of attention.

In this review we present recent developments in spin transport in graphene-hBN vdW heterostructures and discuss the role of hBN as a gate dielectric substrate and as a tunneling spin injection/detection barrier for graphene spintronic devices. We first focus on the early research on graphene spin valves with conventional SiO_2/Si substrates, and discuss drawbacks of oxide dielectric substrates. Then we give an account of the progress in different techniques developed for fabricating graphene-hBN heterostructures, and chronologically examine the progress in hBN supported graphene spin valves. Next, we describe the drawbacks of various oxide tunnel barriers and discuss the recent emergence of atomically thin layers of hBN as tunnel barriers for improved spin injection and detection in graphene. Finally, we share a few interesting perspectives on the future of spintronics with graphene-hBN heterostructures.

8.2 Spin transport measurements

Spin transport in graphene is usually studied in a nonlocal four-terminal geometry, schematically shown in Fig. 8.1(a). A charge current i is applied between C1-C2 contacts and a nonlocal voltage-drop v is measured across C3-C4 contacts. Usually the nonlocal signal is defined in terms of a nonlocal resistance $R_{\rm nl} = v/i$. A non-zero spin accumulation is created in graphene underneath C1 and C2 due to a spin-polarized current through the ferromagnetic (FM) electrodes entering into graphene, and it diffuses along both positive and negative x-directions. Ideally, the charge current is only present in the local part between C1-C2, therefore, the nonlocal voltage is only due to the spin accumulation diffused outside the charge current path. For spin transport measurements, one needs at least two ferromagnetic electrodes, one for spin injection and one for spin voltage detection. The outer electrodes of C1 and C4 can also be nonmagnetic and serve as reference electrodes. For simplicity of the measurement data analysis, they can be designed far away from the inner electrodes and do not contribute to the spin transport.

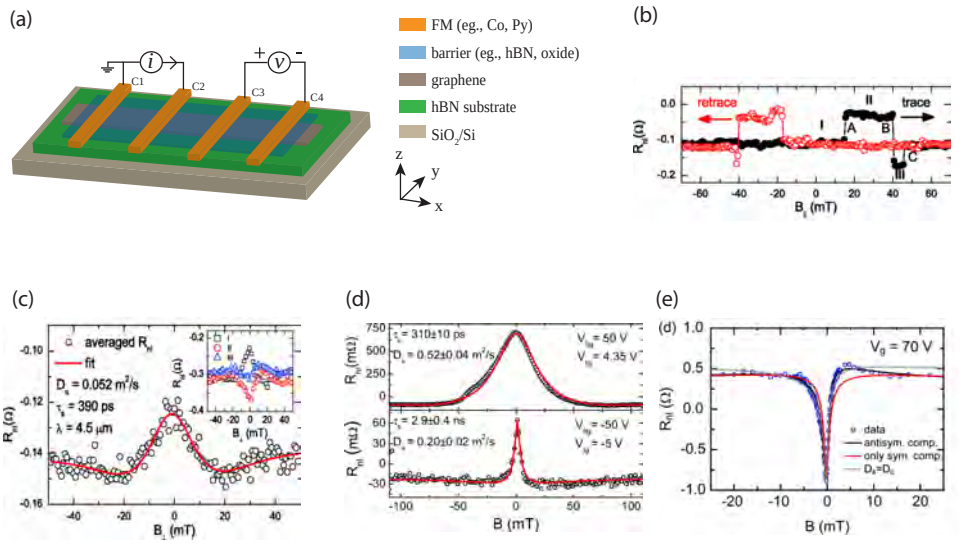

Figure 8.1: Four-terminal non-local characterization of spin transport in hBN dielectric based graphene spin valve devices. (**a**) Schematic of a four-terminal non-local measurement geometry used for spin valve and Hanle spin precession measurements. An AC current i is sourced across a pair of injector contacts and a voltage v is measured across another pair of detector contacts. (**b**) Non-local spin valve signal $R_{\rm nl}$ measured for graphene on hBN substrate [3] [device B1 in Fig. 8.2] as a function of the magnetic field $B_{\rm y}$ applied along the easy axes of the ferromagnetic cobalt electrodes. Magnetization switching of three out of four contacts is denoted by A, B, and C. Hanle spin precession signals $R_{\rm nl}(B_{\rm z})$ measured as a function of the magnetic field $B_{\rm z}$ applied perpendicular to the plane of the spin injection are shown in (**c**) for graphene on hBN substrate [3] [device B1 in Fig. 8.2], (**d**) for graphene encapsulated from the top and the bottom by thick-hBN dielectric [4] [device B2 in Fig. 8.2], and (**e**) for graphene in a bottom-up fabricated device with a large-area top-hBN substrate [5] [device C3 in Fig. 8.2]. Figures (**b**) and (**c**) are reproduced with permission from Ref. [3], ©2012 American Physical Society; (**d**) from Ref. [4], ©2015 American Physical Society; and (**e**) from Ref. [5], ©2016 American Chemical Society.

For spin valve measurements, an in-plane magnetic field $B_{\rm y}$ is applied along the easy axis of the ferromagnets, y-direction[Fig. 8.1(a)]. Initially all the electrodes have their magnetization aligned in the same direction. This configuration is called the parallel (P) configuration. Then $B_{\rm y}$ is applied in the opposite direction. When the magnetization of a FM electrode C2 or C3 reverses its direction, there is a sharp transition registered in v or R_{NL}, and the magnetizations of electrodes in C2-C3 become aligned in the anti-parallel (AP) configuration with respect to each other. On further increasing $B_{\rm y}$, the second electrode also switches its magnetization direction, and now again both electrodes are aligned in P configuration. It completes the spin

valve measurement[Fig. 8.1(b)]. The difference between the magnitude of nonlocal signal in P and AP states, i.e., $\Delta R_{\rm nl} = (R_{\rm nl}^{\rm P} - R_{\rm nl}^{\rm AP})/2$, is termed as nonlocal spin signal or nonlocal magnetoresistance and appears due to the diffusion of the spin-accumulation in the nonlocal part.

The presence of the spin accumulation is confirmed by Hanle spin precession measurements[Figs. 8.1(c-e)]. Here, a magnetic field B_z is applied perpendicular to the plane of graphene. The spins injected via C2 in the x-y plane of graphene precess around B_z and get dephased while diffusing towards C3. The dephasing of the spins is seen in a reduced $\Delta R_{\rm nl}$ as a function of B_z. Spin transport parameters such as spin lifetime $\tau_{\rm s}$, spin diffusion constant $D_{\rm s}$, and spin relaxation length $\lambda_{\rm s}(=\sqrt{D_{\rm s}\tau_{\rm s}})$ are obtained by fitting the Hanle data with the steady state solution to the one-dimensional Bloch equation: $D_{\rm s} \bigtriangledown^2 \vec{\mu_{\rm s}} - \vec{\mu_{\rm s}}/\tau_{\rm s} + \vec{\omega_{\rm L}} \times \vec{\mu_{\rm s}} = 0$, where $\vec{\mu_{\rm s}}$ is the spin accumulation, $\vec{\omega_{\rm L}} = \frac{g\mu_{\rm B}B_z}{\hbar}$ is the Larmor frequency with g=2, the Landé factor, $\mu_{\rm B}$, the Bohr magneton, and $\hbar$, the reduced Planck constant.

The values of $\tau_{\rm s}$ and $D_{\rm s}$ obtained from the spin transport measurements are often used for identifying the spin relaxation mechanism in graphene [3, 6–8]. There are two possible mechanisms that are believed to cause spin relaxation in graphene. One is the Elliott-Yafet (EY) mechanism [9, 10] in which the electron spins relax via the momentum scattering at impurities/defects and as a result $\tau_{\rm s}$ is proportional to the momentum relaxation time $\tau_{\rm p}$. The other one is the D'Yakanov-Perel' (DP) mechanism [11] in which the electron spins dephase in between the two scattering events under the influence of local spin-orbit fields and $\tau_{\rm s}$ is inversely proportional to $\tau_{\rm p}$.

8.3 Challenges due to conventional oxide substrates

Due to the 2D nature of single layer graphene, its carrier density is confined within one atomic thickness, making its surface extremely susceptible to the surroundings. This sensitivity of graphene poses a big challenge while measuring its intrinsic properties. On the other hand, at the same time, the sensitivity is valuable for incorporating physical properties via proximity effects that do not exist in pristine graphene in the first place [12, 13].

In order to make a field-effect transistor (FET), one needs a dielectric environment. The presence of a substrate is necessary to support graphene and to make it useful for device applications. However, the environment that comes with the substrate plays a crucial role in determining the electronic transport properties of graphene.

The ability to image the atomically thick regions of graphene on a SiO_2 surface using an optical microscope led to the discovery of monolayer graphene [14]. Very soon after the discovery, the pioneering work of Tombros *et al.* [15] first demonstrated the electrical spin injection and detection in the non-local four-terminal geometry over a micrometer distance in a monolayer graphene on a SiO_2/Si substrate at room

temperature (RT) [device A1 in Fig. 8.2]. It was further proved by the Hanle spin precession measurements that the spin signal was indeed due to the transport of electron spins in graphene.

The charge and spin transport characteristics of the early reported graphene spin valve devices on SiO_2/Si substrate viz., mobility μ below 5000 $cm^2V^{-1}s^{-1}$, spin lifetime τ_s below 500 ps, and spin relaxation length λ_s up to 2 µm [15, 16], were several orders of magnitude lower than the predicted values $\tau_s \approx 1$ µs and $\lambda_s \approx 100$ µm [1, 2]. Such low values were believed to be due to extrinsic impurity scattering introduced during the device preparation, and the underlying SiO_2/Si substrate. Similar experimental observations were reported subsequently [16–20], and pointed out that the charge impurities and adatoms on SiO_2/Si substrate are the possible sources of an enhanced spin scattering in graphene.

The SiO_2/Si substrate is shown to degrade the electronic quality of graphene due to i)corrugations imparted by its surface roughness, ii)scattering induced from impurity charge traps in oxide [21, 22], iii)surface phonons causing a weak temperature dependent spin relaxation [23], and iv)electron-hole puddles due to charge impurity disorder on the substrate [24, 25]. These observations suggest that, besides the impurities, the underlying SiO_2/Si dielectric substrate also affects the pristine charge and spin transport properties of graphene.

Several attempts have been made to improve the graphene spin valve device architecture for overcoming the aforementioned challenges due to a SiO_2/Si substrate. An account of various device geometries developed over the past decade is given in Fig. 8.2. In order to avoid impurities and disorder coming from the underlying SiO_2/Si substrate, either it should be removed or replaced. One way to completely remove the influence of the substrate is to suspend graphene [device C2 in Fig. 8.2] which resulted in a very high mobility ($\sim 10^5$ $cm^2V^{-1}s^{-1}$) devices [26]. However, the suspended regions are subjected to ripples and strain [27], and are very delicate, causing fabrication challenges. Spin transport in these devices is limited by the polymer supported regions of the suspended graphene resulting in $\tau_s \approx 120 - 250$ ps and $\lambda_s \approx 1.9 - 4.7$ µm [28, 29]. Another way to overcome the imperfections of SiO_2/Si is to epitaxially grow graphene directly on a substrate such as silicon carbide (SiC) [30, 31][device C1 in Fig. 8.2]. However, the localized states present in SiC were found to influence the spin diffusion transport through interlayer hopping mechanisms [32].

Over the past years few other substrates have also been used for graphene spin valve devices to add additional functionalities to graphene. These include, a $SrTiO_3$ (STO) substrate for an epitaxial growth of highly spin polarized $La_{0.67}Sr_{0.33}MnO_3$ (LSMO) contacts for graphene [33], a $Y_3Fe_2(FeO_4)_3$ (YIG) substrate as a magnetically proximity coupling ferromagnetic insulator [34, 35], and recently used transition metal dichalcogenide (TMDC) substrates to proximity induce spin-orbit coupling in graphene [36–47].

Among all the different substrates proposed for studying spin transport in graph-

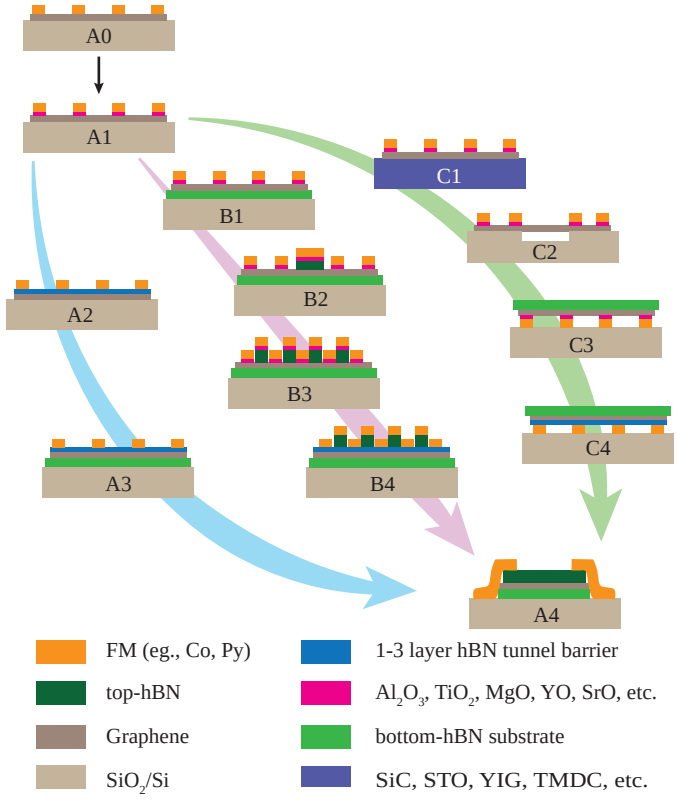

Figure 8.2: Progress in device architecture towards graphene-hBN heterostructures for probing the electrical spin transport in graphene. Early spin transport measurements in graphene were performed using a device geometry (A0) with FM/graphene transparent contacts. Next, tunnel barriers were introduced into the spin valve structures (A1). From there onwards, the progress in the device architecture can be divided into three categories, indicated by three arrows.Spin injection and detection polarizations enhanced with atomically thin hBN tunnel barriers represented via route A1-A2-A3. Improvement in the quality of graphene by encapsulating with thick-hBN dielectrics from the top and bottom is represented via route A1-B1-B2-B3-B4-A4, and by using different substrate environments is represented via route A1-C1-C2-C3-C4. In all the devices except A1, C1, and C2, hBN is used for different purposes such as substrate (A3-A4, B1-B4, C3-C4), top-gate (B2-B4), and tunnel barrier (A2-A3, B4, C4). Legends denote different materials used for fabricating the devices. These device geometries have been used in many studies, for example, A0 in Refs. [48–51], A1 in Refs. [6, 7, 15–19, 52–64], A2 in Refs. [65–70], A3 in Refs. [8, 71, 72], A4 in Ref. [73], B1 in Ref. [3], B2 in Refs. [4, 74, 75], B3 in Ref. [76], C1 in Refs. [30–34, 42], C2 in Refs. [28, 29], C3 in Refs. [5, 77, 78], and B4 and C4 are the proposed new geometries.

ene, it was found that a few nanometer thick hBN can serve as an excellent dielectric substrate to overcome some of the aforementioned problems are for improving the transport characteristics and studying the intrinsic properties of graphene. Atomically thin hBN belongs to the 2D family of layered materials and is an isomorph of graphite with similar hexagonal layered structure with a small lattice mismatch [79] of $\sim 1.8\%$. It is an insulator with a wide bandgap [80] ~ 5.7 eV and can be exfoliated from boron nitride crystals down to a monolayer [81, 82], similar to graphene. In contrast to SiO_2/Si substrates, the surface of hBN is atomically smooth, has few charge inhomogeneities [83], is chemically inert, free of dangling bonds due to a strong in plane bonding of the hexagonal structure, and exerts less strain on graphene [84]. Moreover, the dielectric properties [85, 86] of hBN including a dielectric constant ~ 4 and a breakdown voltage ~ 1.2 Vnm^{-1}, are comparable to SiO_2, favouring the use of hBN as an alternative substrate without the loss of dielectric functionality.

Indeed, among the 2D materials, hBN has been demonstrated to be an excellent dielectric substrate for graphene field-effect transistors [87–90] and spin valves [3, 4, 74, 77], showing excellent charge and spin transport characteristics where graphene on hBN showed very high electronic quality with mobility reaching up to $\sim$ 15,000-60,000 cm^{2}V^{-1}s^{-1} [87, 91][device B1 in Fig. 8.2] and enhanced spin transport parameters: spin lifetime $\tau_s \sim$ 2-12.6 ns [5] and spin relaxation length $\lambda_s \sim$ 12-30.5 µm [4, 5, 74].

8.4 Fabrication: graphene-hBN heterostructures

In order to utilize the aforementioned excellent substrate properties of hBN, one needs to be able to place graphene on the surface of hBN.Various methods have been developed for transferring graphene onto other 2D materials or substrates. These methods can be classified into two categories; methods that require the growth of graphene directly on top of other 2D materials or substrates, and methods that require the transfer of graphene from one substrate to on top of desired 2D materials or substrates. The former methods are of considerable interest for batch production and is still under developing stage for device applications [92–95]. The latter methods have been developed at laboratory scales and are currently in use for fabricating vdW heterostructure devices combining various 2D materials. Here we briefly review the progress in developing the transfer methods for fabricating graphene-hBN vdW heterostructures[Fig. 8.2] for spin transport studies.

The possibility of transferring the exfoliated graphene from a SiO_2/Si substrate to other substrates was first demonstrated by Reina *et al.* [96]. The first reported 2D heterostructure device, a graphene field-effect transistor on hBN, was fabricated by Dean *et al.* [87] by transferring an exfoliated graphene flake onto an exfoliated hBN flake. This method involves the exfoliation of graphene onto a polymer stack, polymethyl-methacrylate (PMMA)/water-soluble-layer(aquaSAVE), followed by dis-

solving the water soluble layer in a DI water bath before transferring onto a hBN substrate, and is thus referred to as "polymer transfer method". To achieve high quality of graphene, it is important to protect its surface from coming in a contact with any solvent. Therefore, the same authors [87] later improved this method to avoid any possible contact with water by replacing the water-soluble-layer with a polyvinyl chloride (PVC) layer which allowed to peel off the PMMA layer without the need to expose graphene/PMMA to water and thereby achieving a fully "dry transfer method" [97]. In a dry transfer method, the interfaces, except the top surface, do not come in a contact with the lithography polymers or any solvents used during the device preparation. However, the polymer contact with a graphene or hBN flake leaves residues which need to be removed by a thermal annealing step, typically in an intert Ar/H_2 atmosphere at 300 °C [87] or in Ar/O_2 at 500 °C [98] for a few hours.

In order to prepare multilayer (>2 layer) heterostructures, a layer-by-layer transfer method [99] was proposed which is equivalent to repeating the dry transfer step [97] followed by the annealing step for transfer of each layer. This layer-by-layer stacking method in principle lacks the control over the crystallographic orientation of the crystals. Moreover, it results in bubbles, wrinkles, and leaves some unavoidable adsorbates at the interfaces of the staked layers which deteriorate the intrinsic quality of the heterostructure. Even during the device fabrication process, the regions of graphene for metallization get exposed to the lithography polymers and leave some residues which are difficult to remove, resulting in low quality electrode-graphene interfaces [99, 100].

The presence of bubbles and wrinkles in a hBN-graphene-hBN heterostructure device [101] limits the mobility of the graphene flake [102]. The problems with folds and bubbles in graphene on hBN can be reduced by using a transfer technique with the aid of an optical mask, developed by Zomer *et al.* [91], using which only up to 5% region of the transferred graphene flakes showed bubbles or wrinkles. The spin valve devices prepared using this method [3] showed an enhanced charge-carrier diffusion with mobilities up to 40,000 $cm^2V^{-1}s^{-1}$ and spin transport signatures over lengths up to 20 µm. This method requires the exfoliation of graphene onto a polymer mask before transferring onto a targeted substrate. The method was later tested by Leon *et al.* [103] with a slight modification, where the graphene flake on a polymer coated substrate can be transferred onto a desired location on another substrate. One drawback of these methods [91, 103] is the difficulty in finding graphene flakes exfoliated on the polymer layer. Moreover the presence of bubbles and wrinkles, due to multiple transfer-annealing processes in a graphene-hBN device [101] limits the graphene mobility [102] and the quality of the electrode interface with graphene [104, 105].

For the assembly of multiple graphene and hBN layers, without exposing the interfaces to polymers and for minimizing the interfacial bubbles, Wang *et al.* [106] developed the "vdW transfer method" in which one hBN flake on a polymer layer

is used for picking up other 2D materials on SiO_2/Si substrates via van der Waals interactions which is stronger between hBN and graphene than that between graphene and SiO_2, or hBN and SiO_2. The graphene channel region encapsulated between the top and bottom hBN flakes does not come in a contact with any polymer, limiting the interfacial bubbles and does not require the annealing step unlike previously reported encapsulated graphene devices [99, 103]. However, this method is useful only for fabricating 1D contacts along the edges of graphene[device A4 in Fig. 8.2], and the 1D ferromagnetic contacts [73, 107] are yet to be proven suitable for fabricating spintronic devices over the traditionally used (2D) ferromagnetic tunnel contacts [15, 71]. Moreover this method is ineffective for picking up graphene flakes longer than the top-hBN flake on the polymer layer.

Later, Zomer *et al.* [108] developed the "fast pick up and transfer method" using which one can make high quality, hBN-encapsulated graphene devices without any size restrictions for a successive pick up of 2D crystals. This method is successfully implemented to fabricate hBN-encapsulated graphene spin valve devices which have demonstrated a long spin lifetime up to 2.4 (1.9) ns in monolayer graphene and 2.5 (2.9) ns in bilayer graphene at RT (4.2 K), and spin relaxation lengths up to 12.1 (12.3) µm in monolayer graphene [74], and 13 (24) µm in bilayer graphene [4] at RT (4.2 K). This method is also used for preparing fully hBN encapsulated graphene spin valve devices [71, 72].

Over the past years few other pick-up and transfer techniques have also been developed for fabricating 2D vdW heterostructures which can be used for preparing graphene spin valve devices depending on the device geometry and material type requirements. These include a "hot pick up technique" for batch assembly of 2D crystals [109], a "deterministic transfer" of 2D crystals by all-dry viscoelastic stamping [110], a "dry PMMA transfer" of flakes using a heating/cooling system for bubble-free interfaces [111], and a "dry-transfer technique combined with thermal annealing" [112].

8.5 hBN as a dielectric substrate for graphene spin valves

The possibility of fabricating graphene-hBN heterostructures by utilizing the aforementioned fabrication techniques enabled the researchers to explore the intrinsic transport properties of graphene in a high quality environment.Due to a smoother surface and less trapped charge impurities than a SiO_2/Si substrate [83], a hBN substrate provides an improved carrier transport in graphene with large mobility [87] and is expected to show enhanced spin transport [24]. The first reported charge transport characteristics of graphene on a hBN substrate showed high mobility $\approx$ 140,000 $cm^2V^{-1}s^{-1}$ which is typically two orders of magnitude higher than in graphene on SiO_2, and the charge neutrality point close to zero gate voltage [87]. Therefore, the

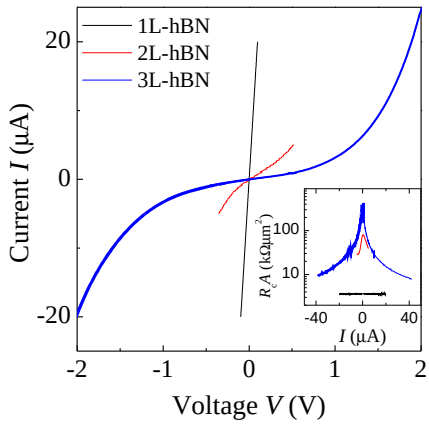

Figure 8.3: Three-terminal I-V characterization of ferromagnetic contacts with a hBN tunnel barrier. I-V characterization of the ferromagnetic contacts with mono, bi, and tri-layers (1L, 2L, and 3L, respectively) of exfoliated-hBN tunnel barriers having thicknesses obtained from the atomic force microscopy (AFM) are 0.52 nm, 0.7 nm, and 1.2 nm, respectively. The inset shows the three-terminal differential contact resistance-area product R_cA as a function of the DC current bias I applied across the contact. Data for 1L-hBN is reproduced with permission from Ref. [71], ©2016 American Physical Society; 2L-hBN from Ref. [72], ©2017 Nature Publishing Group; and 3L-hBN from Ref. [113].

effect of charge impurities on spin transport in graphene is estimated to be lower for graphene on hBN [24].

The first graphene spin valves fabricated on a hBN substrate by Zomer *et al.* [3][Figs. 8.1(b)-8.1(c)] showed an improved charge transport with high mobility $\approx$ 40,000 $cm^2V^{-1}s^{-1}$ and an enhanced spin relaxation length up to 4.5 μm at RT [device B1 in Fig. 8.2]. Moreover, spin signals over a long distance up to 20 μm were also detected. Despite increasing the mobility of graphene, there seemed to be no significant effect of using a hBN substrate on the spin relaxation time whose values are of similar order of magnitude to that is observed using a SiO_2/Si substrate [15, 16, 18]. A study of spin transport in graphene with different mobilities agrees with these results [57]. Therefore, it implies that there is no strong correlation between the observed τ_s and the mobility of the graphene. It also suggests that there is no major role of charge scattering due to substrate in modifying the spin relaxation time.

Even though the hBN substrate provides a smooth and impurity free environment for the bottom surface of graphene, the top surface gets exposed to the chemicals from the device fabrication steps, similar to the devices prepared on a SiO_2/Si substrate [3]. A possible dominant spin relaxation source in this geometry[device B1 in Fig. 8.2] is believed to be the spin scattering due to residues from the polymer assisted fabrication

steps [114], and charge impurities and adatoms already present on graphene. Similar spin relaxation times were observed in graphene on SiO_2/Si and hBN substrates, which indicate that the substrate and its roughness do not seem to drastically influence the spin relaxation in graphene. It was also shown that the EY and DP spin relaxation mechanisms play equally important roles for causing spin dephasing in graphene on hBN as well as in graphene on SiO_2 [3].

The polymer residues and other contaminations due to the sample fabrication can be mechanically cleaned from the graphene on hBN substrate by scanning an AFM tip in contact-mode which sweeps the impurities from the graphene surface [102, 115]. However, during this process ferromagnetic electrodes get exposed to air and may oxidize. In order to avoid the lithography residues on a graphene spin transport channel, while still using the conventional oxide tunnel barriers, two possible routes have been explored over the years; one is the bottom-up fabrication method [77][device C3 in Fig. 8.2] and the other is the encapsulation of graphene from both top and bottom [4, 74][device B2 in Fig. 8.2].

The first route is to reverse the traditional top-down device fabrication process by transferring a hBN/graphene stack on top of the already deposited oxide-barrier/FM electrods on a substrate, as demonstrated by Drögeler *et al.* [77] [device C3 in Fig. 8.2]. This bottom-up approach serves two advantages. First, unlike graphene spin valves prepared via the traditional top-down approach on SiO_2 [15] or hBN [3] substrates, in this method graphene does not come in a direct contact with the lithography polymer PMMA during the device fabrication. Another advantage is that the fabrication procedure does not involve the direct growth of oxide tunnel barriers on graphene which is believed to cause an island growth and subsequent pinholes in the barrier [53], acting as spin dephasing centers. Instead here the MgO barrier is grown epitaxially on cobalt [116], giving a smoother surface [117] for graphene to be transferred directly on top. Due to a high quality interface of the barrier with graphene and its lithography free environment, the resulting mobility values exceeded 20,000 $cm^2V^{-1}s^{-1}$ and spin relaxation time up to 3.7 ns are achieved in a trilayer graphene encapsulated by the hBN from the top [77].

Previously, bilayer graphene spin valve devices on SiO_2/Si substrate [19] have showen the spin relaxation times up to 30 ps for the mobility up to 8000 $cm^2V^{-1}s^{-1}$, and up to 1 ns for the mobility as low as 300 $cm^2V^{-1}s^{-1}$. Whereas the spin lifetime of 3.7 ns was obtained [77] for the devices with mobility of two orders of magnitude higher, 20,000 $cm^2V^{-1}s^{-1}$. The increase in mobility of graphene in the bottom-up fabricated device is attributed to the decoupling of graphene from the SiO_2, while the increase in the spin lifetime is attributed to a clean graphene/MgO contact interface by transferring the graphene directly onto the pre-patterned tunneling electrodes [77, 117]. Later it was discovered that while fabricating a bottom-up device, the lithography solvents can still reach the graphene/MgO contacts region underneath the top-hBN encapsulating flake [5]. The contaminations coming from the solvent

during the device fabrication were found to play substantial role in influencing the spin lifetime. Therefore, when a large-hBN flake was used to avoid graphene from coming in a contact with the solvent, contacts with similar contact resistance-area product R_cA values resulted in a spin lifetime of an order of magnitude higher [5], up to 12.6 ns, compared to the previously reported bottom-up fabricated device [77][Fig. 8.1(e)]. These results indicate that the lithographic impurities are the main limiting factor for spin transport in graphene.

Another route to avoid the polymer contaminations on graphene supported on a hBN is to protect the graphene spin transport channel by encapsulating it from the top with a second hBN flake[device B2 in Fig. 8.2]. The top-hBN encapsulation layer serves few advantages: (i)it protects the graphene transport channel from coming in a direct contact with the lithography polymers or solvents [74], (ii)it can be used as a top-gate dielectric to tune the carrier density in the encapsulated graphene transport channel and create $p-n$ junctions [71], and allows to study spin transport across the $p-n$ junction [71, 76, 118], and (iii)it creates the possibility to electrically control the spin information in graphene via Rashba SOC [74].

Guimarães *et al.* [74] fabricated a spin valve device in which the central part of the graphene flake on a hBN substrate is covered with a top-hBN flake[device B2 in Fig. 8.2]. The encapsulated region showed large mobility up to 15,000 $cm^2V^{-1}s^{-1}$ at RT, and resulted in an enhanced spin lifetime about 2 ns and spin relaxation length about 12 µm for a monolayer-graphene [74] [Fig. 8.1(d)] at RT. This is a combined effect of an improved carrier transport (D_s) and spin relaxation time. However the nonecapsulated region showed a spin lifetime around 0.3 ns in the same flake [74], similar to the case of bare graphene on hBN [3].In this device geometry[device B2 in Fig. 8.2], the spin transport channel also consists of nonencapsulated regions where graphene is exposed to the polymer residues on outside of the top-hBN, with mobilities and spin relaxation times lower than the top-hBN encapsulated region [4, 74]. Such an unevenly doped graphene channel makes it difficult to analyse the spin transport measurements in the central region [4, 28, 74, 75] and requires complex modeling.

Further understanding about the influence of the polymer residues on spin transport properties can be achieved by reducing the size of the graphene regions exposed to the polymer residues. Avsar *et al.* [76] studied the role of extrinsic polymer residues on the spin relaxation in bilayer-graphene encapsulated everywhere except under the contacts by a pre-patterned thick top-hBN layer and a bottom-hBN substrate[device B3 in Fig. 8.2]. The authors reported a nearly five times higher τ_s of $\approx$ 420 ps for the hBN encapsulated regions compared to τ_s of $\approx$ 90 ps for the non-encapsulated regions of the same device. It suggests that the lithographic residues on the spin transport channel have a significant effect on the spin transport properties. The reported $\tau_s \approx$ 90 ps for the non-encapsulated graphene is comparable to that for bare graphene on SiO_2 [15] and hBN [3] substrates with similar mobilities. It supports the conclusions

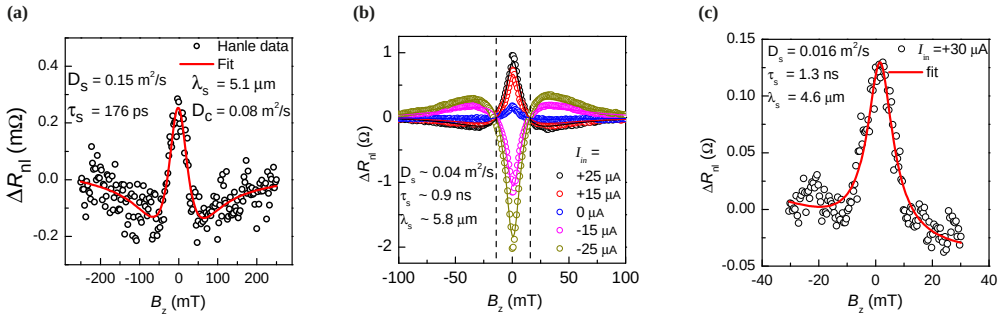

Figure 8.4: Four-terminal non-local Hanle spin precession measurements using ferromagnetic contacts with atomically thin layers of exfoliated-hBN tunnel barriers. Hanle signals $\Delta R_{\rm nl}$ in (**a**), (**b**), and (**c**) are measured in fully hBN encapsulated graphene devices with a thick bottom-hBN substrate and a top monolayer, bilayer, and trilayer-hBN tunnel barriers, respectively, as a function of the magnetic field B_z applied perpendicular to the plane of the spin injection. $\Delta R_{\rm nl}(B_z) = (R^{\rm P}_{\rm nl}(B_z) - R^{\rm AP}_{\rm nl}(B_z))/2$ where $R^{\rm P(AP)}_{\rm nl}(B_z)$ is the non-local resistance measured as a function of B_z when the relative magnetization of the injector and detector contacts is aligned in a parallel, P(anti-parallel, AP) configuration. Solid lines represent the fits to the data using the one-dimensional solution to the Bloch equation, and the corresponding fitting parameters $D_{\rm s}$, $\tau_{\rm s}$, and $\lambda_{\rm s}$ ($=\sqrt{D_{\rm s}\tau_{\rm s}}$) are given in each figure. No bias applied for the measurement shown in (**a**). The applied injection current bias $I_{\rm in}$ values are given in the legend for (**b**) and (**c**). Note that the sign reversal of the Hanle signal for the device with bilayer-hBN barrier is due to the inverse spin injection polarization of the injector for negative bias. Hanle signal for the device with trilayer-hBN is measured at $I_{\rm in}$ = +30 μA. Figure (**a**) is reproduced with permission from Ref. [71], ©2016 American Physical Society; (**b**) from Ref. [72], ©2017 Nature Publishing Group; and (**c**) from Ref. [113].

of Zomer *et al.* [3] that the impurities, surface phonons, and roughness of the underlying substrate are not the limiting factors of spin relaxation in graphene. Therefore, low values of spin transport parameters can be attributed to the contact regions of graphene that are exposed to polymers and the quality of the oxide tunnel barrier interface with graphene.

One needs to find a way to avoid the polymer contaminations on graphene, even underneath the contacts. This improves the tunnel barrier interface with graphene. In principle, both can be achieved by fully encapsulating the graphene spin transport channel from the top and bottom.However, one of the encapsulating layers needs to be of only few atomic layers thick, so that it can also be used as a tunnel barrier for electrical spin injection and detection via the ferromagnetic electrodes. In fact, atomically thin hBN was found to be a unique tunnel barrier for graphene field-effect transistor devices [88] in additional to its excellent dielectric substrate properties. Moreover, the full encapsulation of graphene with hBN by far has proved to be

effective for an efficient spin injection/detection in graphene which will be discussed in Section 8.7.

8.6 Challenges due to conventional oxide tunnel barriers

So far we have been discussing the effect of the quality of graphene over its spin transport and the progressive improvement by adapting various graphene-hBN heterostructure device geometries, viz., devices A1, A2, A4, B1-B3, and C1-C3 in Fig. 8.2. Another factor, which is believed to be a major cause of spin relaxation in graphene, that we have not discussed so far, is the spin relaxation due to the ferromagnetic tunneling spin injection and detection contacts, and their interface with the underlying graphene.

In a basic graphene spin valve device [device A0 in Fig. 8.2],a charge current passing through an FM/graphene contact can create a spin accumulation in graphene underneath the contact. Signatures of nonlocal spin injection and detection in graphene through FM/graphene transparent contacts [device A0 in Fig. 8.2] have been reported in early spin transport investigations [48–51]. However, due to the well known conductivity-mismatch problem [119] with these contacts there is spin absorption and spin relaxation via the ferromagnetic electrodes, and the efficiency of spin injection into graphene is reduced [120].

The fundamental problem of spin injection which is the conductiviy mismatch problem, was first highlighted by Filip *et al.* [119] for spin injection into semiconductors, according to whom comparable resistivities of the ferromagnetic metal electrode and graphene lead to a negligible spin injection polarization in graphene. The solution to this problem, according to Rashba [121], and Fert and Jaffrès [122], is to introduce a highly resistive tunnel barrier at the FM-graphene interface which will limit the back flow of the spins from graphene into the FM, and avoid the contact induced spin relaxation. Therefore, the first experimentally reported unambiguous nonlocal spin transport via Hanle spin precession measurements in graphene spin valve devices was achieved by using Al_2O_3 tunnel barriers between the FM and graphene [15] i.e., with FM/Al_2O_3/graphene tunnel contacts. Even though the Hanle spin precession signal was also measured later with transparent contacts [120], the spin injection efficiency was highly limited by the conductivity mismatch problem [18, 54, 120].

In spite of introducing the thin layer of oxide tunnel barriers, the metrics for spin transport in graphene, i.e., spin lifetime and spin relaxation length, are far lower than the estimated values for intrinsic graphene [1, 123, 124]. These values are believed to suffer from the combined effect of the quality of the tunnel barrier, and its interface with graphene, besides the impurities present in the transport channel.

Now we chronologically review the progress of oxide tunnel barriers for spin

injection and detection in graphene.Overall, the spin relaxation time in graphene is limited by the ferromagnetic tunnel contacts in two ways. One way is through spin absorption from graphene into FM electrodes via pinholes in the tunnel barrier. The pinholes provide a short circuit path between the FM electrode and graphene, leading to the conductivity mismatch problem [119]. This effect can be quantified with the values of $(\frac{R_c}{R_s}, \frac{L}{\lambda})$ parameters [63, 125–127], where R_c is the contact resistance, R_s is the spin resistance of graphene, and $R_s = \frac{R_{sq}\lambda_s}{W}$ with the square resistance R_{sq} and width W of graphene. Even when there is no conductivity mismatch problem, there can still be an influence of contacts on the spin transport properties of the transport channel. Another way to influence the spin relaxation time is through the multiple tunnel barrier-graphene interface related effects such as a deteriorated graphene surface due to a direct deposition of the barrier material which can lead to an island like growth of oxide barrier and amorphize graphene where the barrier is grown [56], magnetostatic fringe fields from ferromagnets [128], spin-flip scattering at the nonuniform interface between the barrier and graphene [129–131] and and a complex interplay between ferromagnet d-orbitals and graphene π-orbitals [59, 132].

Over the past years, much of the research is dedicated to understand the potential sources of spin relaxation in graphene with respect to ferromagnetic tunnel contacts, especially the role of oxide barriers. It has focused on two aspects of the tunnel barriers. One is the material type, for example, Al_2O_3, MgO, TiO_2, and SrO. The other one is the growth method, for example, electron beam evaporation, atomic layer deposition (ALD), molecular beam epitaxy (MBE) growth, and sputtering.

Several studies have revealed that, in case of oxide barriers, besides the choice of the barrier material, the method of evaporation or growth of the barrier is also important to achieve an efficient spin injection. Tunnel barriers of Al_2O_3 grown by Tombros *et al.* [15] involve the deposition of Al by the electron beam evaporation at first, followed by the oxidation step which likely gives pinholes in the barrier as reported in subsequent reports from the same group [17, 18]. The spin lifetime is observed to be increased with TiO_2 barriers [3, 15] grown by electron beam evaporation which are believed to be smoother than Al_2O_3 barriers. However, there has been no systematic investigation of the growth and quality of TiO_2 barriers in relation to the spin relaxation time in graphene.

Early results on spin injection with MgO barriers grown by electron beam evaporation reported to show pinholes, caused by the high surface diffusivity of MgO on graphene, resulting in the inhomogeneous island growth of MgO on the graphene surface [16, 133]. Dlubak *et al.* [56] showed that the sputtering of MgO causes more damage to the graphene lattice by amorphization of carbon than the sputtering of Al_2O_3. The MBE growth of MgO does not seem to impact the quality of graphene [19], and gives a relatively pinhole free, uniform, and continuous MgO layer on graphene [134]. Despite the presence of occasional pinholes in these MgO barriers, Yang *et al.*

[19] reported long spin relaxation times up to 2 ns in exfoliated bilayer graphene on a SiO_2/Si substrate. However, the tunneling characteristics and spin injection efficiency of these contacts were not discussed by the authors. A direct observation of increase in the spin lifetime with an increase in contact resistance-area R_cA product of the MgO barrier contacts indicates that the pinholes in the barrier contacts significantly affect the spin relaxation in graphene underneath the contacts [59]. Furthermore, by successive oxygen treatments, low-R_cA MgO contacts with transparent regions or pinholes can be successfully transformed into high-R_cA contacts with a reduced pinhole density [132]. Such behaviour of the contacts suggests that the spin lifetime and spin injection efficiency are limited by the presence of pinholes in the barrier.

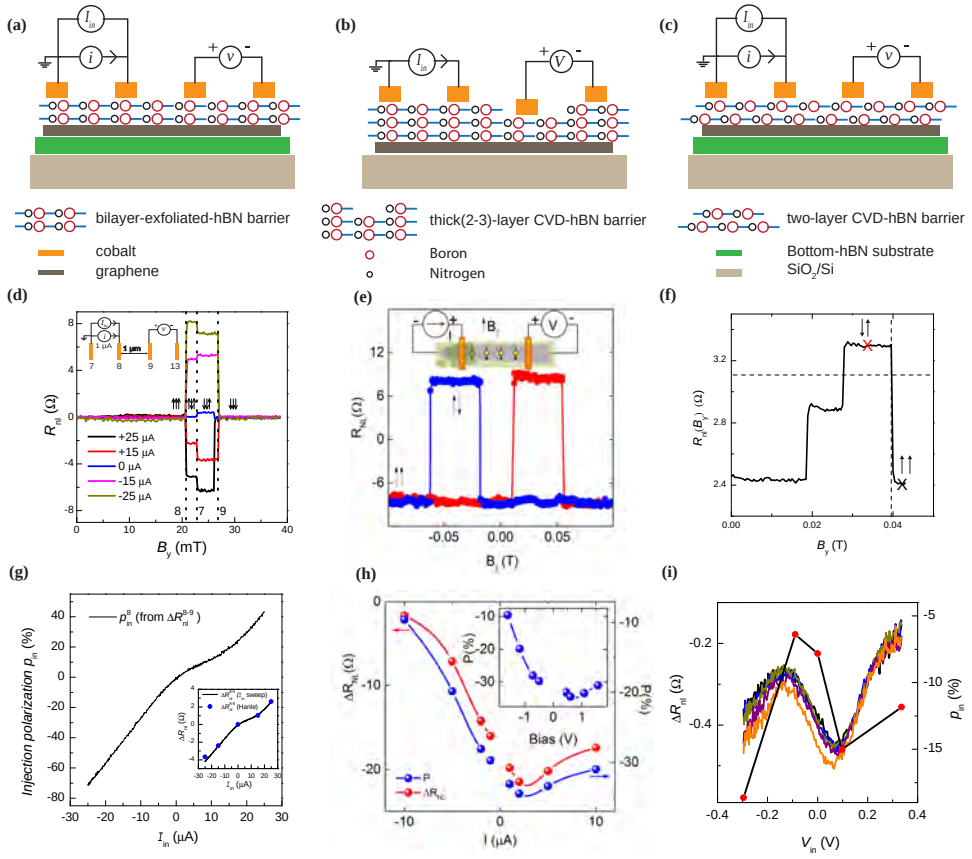

Figure 8.5: Bias induced non-local spin signal and spin injection polarization using the ferromagnetic tunnel contacts with bilayer-exfoliated-hBN, thick(1-3 layer)-CVD-hBN, and two-layer-CVD-hBN tunnel barriers. (*Caption continued on the next page.*)

Addition of a Ti buffer layer between MgO and graphene has been shown to curb

Figure 8.5: Schematic of the device geometry for (**a**) a fully hBN encapsulated graphene with a bottom thick-exfoliated-hBN substrate and a top bilayer-exfoliated-hBN tunnel barrier contacts, (**b**) graphene on a SiO_2/Si substrate with thick(1-3 layer)-CVD-hBN barrier contacts, and (**c**) a fully hBN encapsulated graphene with a bottom thick-exfoliated-hBN substrate and a top two-layer-CVD-hBN barrier. For devices in (**a**) and (**c**), an AC current i is applied across the injector contacts and the non-local voltage v is detected using the standard low-frequency lock-in technique, and the non-local differential resistance $R_{\rm nl} = v/i$ is determined at each desired value of a DC current bias $I_{\rm in}$ applied across the same injector contacts. For device in (**b**), pure DC measurements were performed using a DC current source I and a DC voltmeter V where the non-local DC resistance is $R_{\rm NL} = V/I$. The tunnel barrier in (**a**) is obtained by a mechanical cleaving of crystalline hBN flakes. The tunnel barrier in (**b**) is as-grown by CVD, inhomogeneously, with a variation in thickness of 1-3 layers, whereas the barrier in (**c**) is made by layer-by-layer stacking of two individual monolayers of CVD-hBN. Schematically, the inhomogeneity in as-grown CVD-hBN in (**b**) is depicted by different thickness regions underneath the cobalt electrodes, and the non-crystalline nature of two-layer-CVD-hBN in (**c**) is depicted by a slight vertical misalignment of atoms. (**d**), (**e**), and (**f**) show the four-terminal non-local resistance $R_{\rm nl}$ measured in a spin valve configuration as a function of the magnetic field $B_{\rm y}$ for the devices shown in (**a**), (**b**), and (**c**), respectively. The relative magnetization orientation of the cobalt electrodes is denoted by the *up* (↑) and *down* (↓) arrows. (**g**) shows bias enhanced differential spin injection polarization $p_{\rm in}$ and non-local differential spin signal $\Delta R_{\rm nl} = (R_{\rm nl}^{\rm P} - R_{\rm nl}^{\rm AP})/2$ (inset) as a function of the injection current bias $I_{\rm in}$ (or, equivalent voltage bias $V_{\rm in}$) for the device with bilayer-exfoliated-hBN tunnel barriers. (**h**) shows non-local spin signal $\Delta R_{\rm NL} = R_{\rm NL}^{\rm P} - R_{\rm NL}^{\rm AP}$ and DC spin injection polarization $P_{\rm in}$ (inset) as a function of I and V, respectively, for the device with thick-CVD-hBN tunnel barriers. (**i**) shows $\Delta R_{\rm nl}$ and $p_{\rm in}$ as a function of $V_{\rm in}$ for the device with two-layer-CVD-hBN tunnel barriers. Figures (**d**) and (**g**) are reproduced with permission from Ref. [72], ©2017 Nature Publishing Group; (**e**) and (**h**) from Ref. [69], ©2016 Nature Publishing Group; (**f**) and (**i**) from Ref. [8], ©2018 American Physical Society.

the mobility of surface atoms and allow the growth of an atomically smooth layer of MgO barrier by the MBE [53]. Indeed, TiO_2 seeded MgO barriers were reported [16] to show tunneling characteristics, resulting in large spin polarizations up to 30% and long spin relaxation times up to 500 ps, compared to then previously reported transparent [48–51, 120] and pinhole [18, 54] contacts, indicating a reduction in spin relaxation due to the improved quality of the tunnel contacts [16]. However there was not a good control achieved over the reproducibility of high quality growth of TiO_2 seeded MgO tunnel barriers and it has been difficult to achieve a high spin injection polarization consistently [16].

For an efficient use of MgO barriers and to avoid the contact growth directly on graphene, a new workaround was introduced [77], the 'bottom-up fabrication method'[device C3 in Fig. 8.2], where MgO/Co contacts were first deposited by the MBE on a bare SiO_2/Si substrate followed by transferring the hBN/graphene stack

on top. In addition, this geometry also blocks the polymer residues from coming in contact with graphene at the barrier/graphene interface, and resulted in a high spin relaxation time up to 3.7 ns in trilayer graphene. This performance was attributed to a clean interface of the barrier with graphene and high-R_cA of the contacts. These results imply that the quality and direct growth of the oxide barrier, and the polymer residues at the barrier-graphene interface play an important role in spin dephasing in graphene, especially underneath the contacts.

Over the past years few other tunnel barriers have also been used for graphene spin valve devices. These include a pulsed laser deposition (PLD) growth of ferromagnetic oxide LSMO contacts for graphene on a STO substrate [33], ALD growth of diazonium salt seeded HfO_2 tunnel barrier for epitaxial graphene on SiC substrate [135], thermal evaporation growth of yttrium-oxide (Y-O) barrier for graphene on SiO_2/Si substrate [136], MBE growth of SrO barriers for graphene on SiO_2/Si substrate [137–139], hydrogenated graphene barriers for graphene on a SiO_2/Si substrate [140], fluorinated graphene for graphene on a SiO_2/Si substrate [141], electron-beam induced deposition of amorphous carbon interfacial layer at the FM/graphene interface [142], exfoliated [35, 65, 70–72] and CVD grown [8, 67, 69] hBN barriers for graphene on SiO_2, hBN, and YIG substrates, and exfoliated-TMDC barrier [41] for graphene on a SiO_2 substrate.

8.7 hBN as a tunnel barrier for spin injection and detection in graphene

The aforementioned works highlight the importance of growing a tunnel barrier that is atomically flat, homogeneously covering graphene with a uniform thickness, free from pinholes, devoid of the conductivity mismatch problem, and efficient in injection and detection of spin polarization in graphene. Among all the different tunnel barriers or interfacial layers proposed for studying spin injection in graphene, it was found that a thin layer of atomically flat hBN with a similar lattice structure as graphene can serve as an excellent tunnel barrier to overcome the aforementioned challenges [65, 71, 72, 143].

The promising nature of hBN as a tunnel barrier is revealed from the conductive AFM measurements of electron tunneling through thin layers of hBN [144], where it was shown that mono, bi, and tri-layers of exfoliated-hBN exhibit a homogeneously insulating behaviour across the flakes without any charged impurities and defects. Furthermore the breakdown voltage of hBN was found to increase with the number of layers [144], and the estimated dielectric breakdown strength was found to be [86, 144–147] $\sim$ 0.8-1.2 Vnm^{-1}. These results were further confirmed by Britnell *et al.* [145], who reported that the hBN/graphene interface resistance increases exponentially with the number of hBN layers and the tunneling characteristics as confirmed by a

nonlinear I-V behaviour. These results also demonstrate the potential of atomically thin hBN to be used as ultra smooth and pinhole free tunnel barrier for spin injection into graphene. Moreover, first-principle calculations estimate that the efficiency of spin injection in Ni/hBN/graphene heterostructures can be achieved up to 100% with increasing the number of hBN layers [148].

Yamaguchi *et al.* [65] were the first to experimentally show electrical spin injection and detection through a monolayer exfoliated-hBN tunnel barrier in a bilayer graphene. However, the spin lifetime $\approx$ 56 ps and spin polarization $\approx$ 1-2% are of the same order of magnitude as that of devices with FM/graphene transparent contacts [120]. Besides small hBN crystalline flakes, the chemical vapour deposition (CVD) grown large-area hBN as a tunnel barrier for spin transport studies was also explored by Kamalakar *et al.* [67] and Fu *et al.* [68].

Fu *et al.* [68] studied the spin transport in large-scale devices with CVD-hBN barrier and CVD-graphene transport channel on SiO_2/Si substrates. A monolayer CVD-hBN barrier [68] showed a small spin signal, whose magnitude is similar to that of obtained with a monolayer exfoliated-hBN barrier [65]. A two-layer CVD-hBN barrier [68] resulted in relatively large signals (with polarization $\approx$ 5%). However, the spin life time $\approx$ 260 ps is comparable to the devices with exfoliated or CVD graphene on SiO_2/Si substrate [18, 134].

In a parallel study, Kamalakar *et al.* [67] used CVD-hBN barriers with exfoliated-graphene on SiO_2/Si substrate and reported that hBN can serve as an alternative efficient tunnel barrier by demonstrating an order of magnitude higher spin lifetime $\approx$ 500 ps and enhanced spin polarization $\approx$ 11% compared to then previous attempts with hBN barriers [65, 68]. In another report, the same authors [66] systematically investigated the spin transport in graphene for various R_cA product values of Co/CVD-hBN/graphene contacts ranging from transparent to high resistance, and showed that by increasing R_cA, the spin lifetime enhanced up to 460 ps and spin polarization up to 14%. Also, they were the first ones to observe [69] the novel effect of spin signal inversion by varying the thickness(1-3 layers) of CVD-hBN barriers and the corresponding interface resistance of Co/CVD-hBN/graphene junctions. The enhanced magnitude of the spin polarization up to $\approx$ 65% is an order of magnitude higher compared to then previously reported results with oxide barriers [12, 149] and hBN barriers [65, 68, 71]. Indeed, these results were further improved and confirmed by later efforts from other groups [8, 70–72, 113] in encapsulated graphene, establishing the fact that thicker hBN barriers would result in a larger values of spin lifetime and spin polarization.

A number of reports on spin transport studies in graphene with CVD-hBN tunnel barriers incorporated a bare SiO_2/Si substrate [66–69]. Moreover, the PMMA assisted wet transfer of CVD-hBN could affect the quality of graphene. Therefore, in order to further improve the spin transport parameters while using the CVD-hBN barrier, it was encouraged [66] to use high mobility graphene such as graphene on hBN [3] or

hBN encapsulated graphene [74]. Even though hBN substrate has not been reported to enhance the spin relaxation times in graphene compared to SiO_2/Si substrate [3], it can increase the diffusion constant D_s and thus spin relaxation length λ_s ($=\sqrt{D_s\tau_s}$). Gurram *et al.* [8] studied the electrical spin injection and detection in graphene on a thick-exfoliated-hBN substrate using a layer-by-layer-stacked two-layer-CVD-hBN tunnel barrier [device A3 in Fig. 8.2]. However, the mobility of graphene was found to be below 3400 $cm^2V^{-1}s^{-1}$ and the spin relaxation time lower than 400 ps and are comparable to the values reported by Kamalakar *et al.* [66, 69]. Therefore, such low values of spin transport parameters point to the utmost importance of a clean transfer process using CVD materials.

In order to explore spin injection via hBN barrier in a cleaner environment, one can use the dry pick up and transfer method [108] for fabricating encapsulated graphene devices with exfoliated-hBN flakes. Early attempts to study the spin transport in hBN encapsulated graphene [4, 74][device B2 in Fig. 8.2] resulted in an improved spin relaxation length up to 12 µm and spin lifetime up to 2 ns. Note however that these values correspond to the intrinsic values of the graphene in the hBN encapsulated region, but the effective spin relaxation time of the spin transport channel is reduced by the non-encapsulated regions [4, 28, 74, 75]. It indicates that, perhaps, a complete encapsulation of graphene will improve the spin transport, and provide access to the direct measurement of intrinsic spintronic properties of the encapsulated graphene.

Fully encapsulated graphene with various thick 2D materials has been studied for charge transport characteristics with 1D or quasi-1D contacts [106, 150]. The potential of 1D FM edge contacts[device A4 in Fig. 8.2] has only been recently explored [73, 107] for spin transport studies and these contacts are yet to be proven viable for efficient spin injection/detection in graphene. On the other hand, in order to use the conventional contact geometry, an atomically thin layer of hBN can be used as a top encapsulation layer[device A3 in Fig. 8.2]. The thin-hBN layer can serve two purposes in this device geometry. First, as an encapsulation layer to protect the graphene channel from the lithography impurities, and second, as a tunnel barrier for the electrical spin injection and detection in graphene via ferromagnetic electrodes.

Gurram *et al*. [71] reported spin transport in a new lateral spin valve device geometry[device A3 in Fig. 8.2], where graphene is fully encapsulated between two hBN flakes to overcome the challenges together due to the substrate, the tunnel barrier, and the inhomogeneity that can be introduced during sample preparation. In this device geometry, the charge mobility values ($\approx$ 8200-11800 $cm^2V^{-1}s^{-1}$) lie close to each other for different regions of the encapsulated graphene, implying a uniform charge transport across the graphene flake. Moreover, the spin transport measurements resulted in consistent spin relaxation parameters which do not differ much for different regions in the same device. Such homogeneity is difficult to achieve in the partially hBN-encapsulated graphene device [4, 74, 75] with oxide barriers.

Ferromagnetic tunnel contacts with a low value of R_cA product indicate the trans-

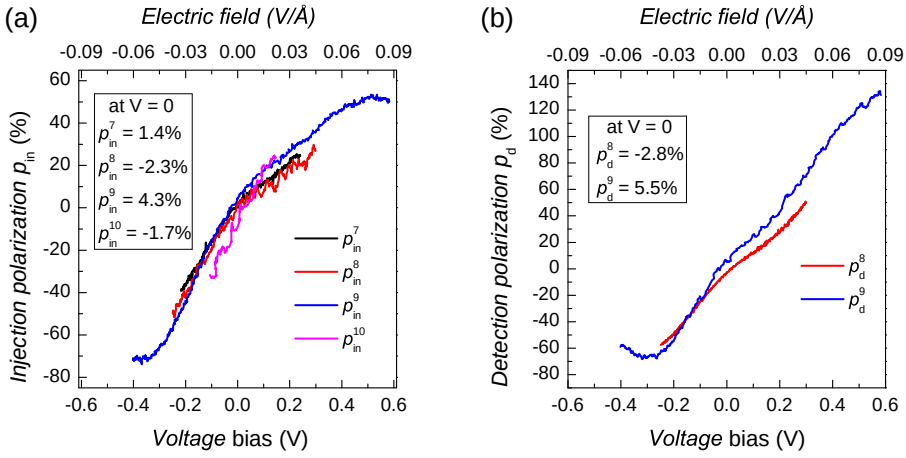

Figure 8.6: Bias induced differential spin-injection (p_{in}) and detection (p_d) polarizations of ferromagnetic tunnel contacts with bilayer-exfoliated-hBN barrier, adopted from Ref. [72]. (**a**) shows p_{in} for four different injector contacts as a function of the DC voltage bias V applied across the injector. (**b**) shows p_d for two different detector contacts as a function of the DC voltage bias V applied across the detector while the injector contacts were biased at I_{in}=+20 µA. Top *x-axes* in (**a**) and (**b**) represent the effective electric field (=V/t, thickness of the bilayer-hBN t≈7 Å) across the contacts. The insets show the polarizations at zero bias. Figures (**a**) and (**b**) are reproduced with permission from Ref. [72], ©2017 Nature Publishing Group.

parent nature of the barriers, generally attributed to the presence of pinholes [125]. Such behaviour is commonly observed with conventional oxide tunnel barriers and, as discussed before, is detrimental to the efficient spin injection due to a possibility of back-flow of the injected spins [63, 125–127]. Moreover, low-R_cA contacts with conventional oxide tunnel barriers are reported to show spin transport only across small length scales which are limited to the injector-detector seperation due to spin absorption via pinholes in the contacts [125]. A fully hBN encapsulated graphene spin valve device [71] showed a long distance spin transport in the monolayer-hBN encapsulated graphene channel up to the length of 12.5 µm, while having multiple low-R_cA contacts [71] in the spin transport channel. Such behaviour was attributed to the combined effect of pinhole free nature of the monolayer-hBN barrier and a clean hBN/graphene interface [71].

Even after fully encapsulating graphene from the top with a monolayer-hBN and from the bottom with a thick-hBN, τ_s of graphene is still lower than 300 ps [65, 71] which is comparable to τ_s in graphene on SiO_2 or hBN [3], and the spin polarization is lower than 2% which is similar to the values obtained with conventional oxide barriers [149]. The limited values of the spin transport parameters are due to the

combined effect of i)low-R_cA values of FM/1L-hBN/graphene contacts resulting in a low spin injection polarization, and ii)the proximity of polymer residues which are only one hBN layer away from graphene that could lead to spin scattering in graphene resulting in a low spin relaxation time. Therefore, increasing the thickness of hBN tunnel barrier should solve the problems due to the conductivity mismatch and the proximity of polymer residues.

According to Britnell *et al.* [145], the R_cA product of contacts can be increased by increasing the number of layers of hBN tunnel barrier which can overcome the conductivity mismatch problem. By doing so, it is also estimated that up to 100% spin polarization can be achieved [148]. On the experimental side, it was demonstrated by Singh *et al*. [70] that bilayer-hBN is a better choice for tunnel barrier than monolayer-hBN in order to achieve longer spin lifetimes exceeding nanoseconds in graphene and higher spin injection polarization values.

8.7.1 Bias induced spin injection and detection polarizations

Biasing ferromagnetic tunnel contacts for spin injection in graphene was predicted to show rich physics in terms of studying spin injection into graphene in the presence of electric field, and potentially inducing magnetic proximity exchange splitting in graphene [151, 152]. The first report on bias dependent spin injection polarization of hBN barriers [69] revealed a large magnitude of polarization up to 65% and also a novel sign inversion behaviour while varying the thickness of CVD-hBN barriers. In a recent experiment, Gurram *et al.* [72] showed that an unprecedented enhancement of differential spin polarization can be achieved by biasing the injector or detector contacts with bilayer-hBN tunnel barriers. The authors [72] reported that the application of bias across FM/bilayer-hBN/graphene/hBN contacts[Fig. 8.5(a)] resulted in surprisingly large values of differential spin injection p_{in} and detection p_d polarizations up to $\pm$100%, and a unique sign inversion of spin polarization as a function of bias, near zero bias. Moreover, unbiased spin polarizations of contacts were found to be both positive and negative[see Fig. 8.6].

Later, same authors report that the bias-dependent p_{in} for high-R_cA contacts with two-layer-stacked-CVD-hBN tunnel barriers [8] was found to be different from the bilayer-hBN barrier [72] in two ways. First, there is no change in sign of p_{in} within the applied DC bias range of $\pm$0.3 V[Fig. 8.5(i)]. Second, the magnitude of p_{in} increases only at higher negative bias close to -0.3 V. This behaviour marks the different nature of bilayer-exfoliated-hBN [72] and two-layer-CVD-hBN [8] tunnel barriers with respect to the spin injection process. Moreover, these results emphasize the importance of the crystallographic orientation of the two layers of hBN tunnel barrier. The bias dependence of the spin polarization is different for different thicknesses of the hBN tunnel barrier [69, 72, 113] and needs to be understood within a proper theoretical framework.

8.7.2 Two-terminal spin valve and Hanle signals

Two-terminal spin injection and detection in a lateral spin valve device geometry is technologically more relevant than in a four-terminal spin valve geometry. Usually, it is difficult to measure spin-dependent signals in a two-terminal geometry either due to the presence of large charge current dependent background signal or due to low efficiency of the spin injector and detector contacts. The first two-terminal spin transport measurements in graphene were reported with permalloy(Py)/graphene transparent contacts [48] followed by three other studies reported with MgO [133] and Al_2O_3 tunnel barriers [15, 31]. However, the magnetoresistance effects could mimic these spin valve signals in the local measurement configuration. Moreover, none of these studies showed an evidence of unambiguous signature of the spin transport in the two-terminal configuration via Hanle spin precession measurements [15].

The recent report [72] showed that the bias-induced spin injection and detection polarizations of bilayer-hBN tunnel barrier contacts [72] are large enough[Fig. 8.6] to be able to detect spin transport in a two-terminal configuration with spin signals reaching up to 800 Ω and magnetoresistance ratio up to 2.7%. Moreover, the authors also observed unambiguous evidence of spin transport in the two-terminal measurement geometry via Hanle spin precession measurements using the bilayer-hBN tunnel barrier contacts [113][Fig. 8.8(b)]. This is the first demonstration of a two-terminal Hanle signal. However, this has been only one experimental report so far and there is a need for more experiments to establish the potential of hBN barriers for two-terminal spin valve applications.

8.7.3 Spin relaxation

Theoretically, Tuan *et al.* [24] studied the spin dynamics and relaxation in clean graphene to understand the effect of substrate induced charge inhomogeneities such as electron-hole puddles on the spin relaxation mechanism. For the case of SiO_2 substrates, the authors numerically demonstrated the presence of the DP mechanism due to random spin dephasing by the eletron-hole puddles. For substrates with less inhomogeneities, such as hBN, spin relaxation for graphene on hBN is caused by substrate induced broadening in the spin precession frequency where τ_s follows τ_p. For higher τ_p, spins relax under the influence of substrate induced Rashba spin-orbit coupling. Therefore, for a graphene on hBN susbstrate, spin relaxation is expected by the energy broadening and due to the substrate-induced SOC rather than under the influence of the impurities.Experimentally, Zomer *et al.* [3] studied the spin relaxation in relation to the quality of graphene on hBN device which is contaminated with the polymer residues on the top-surface of graphene[Fig. 8.7(a)]. The authors [3] show that the spin transport data is best described by the equal contributions of EY and DP

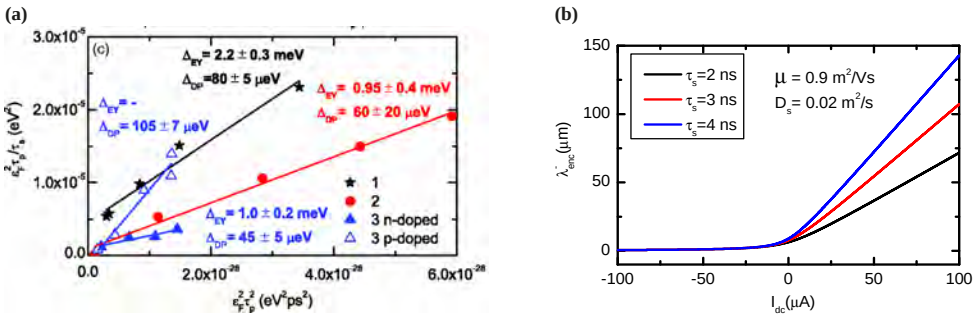

Figure 8.7: Spin-relaxation and spin-drift in graphene-hBN heterostructures. (**a**) Investigation of spin relaxation in a high mobility graphene on a hBN substrate. The possibility of the Elliott-Yafet (EY) and D'yakonov-Perel' (DP) mechanisms is explained by following the relation between τ_s and momentum relaxation time τ_p, $\frac{\varepsilon_F^2 \tau_p}{\tau_s} = \Delta_{EY}^2 + \left(\frac{4\Delta_{DP}^2}{\hbar^2}\right)\varepsilon_F^2 \tau_p^2$, where, ε_F is the Fermi energy, and $\Delta_{EY(DP)}$ is the effective spin-orbit coupling strength of EY(DP) mechanism, whose value is obtained from the linear fitting. The respective relaxation rates are found to be of similar order of magnitude for both the EY and DP, indicating no clear dominance of either of the mechanisms. (**b**) shows a strong modulation of the spin relaxation length as a function of the drift current in a high mobility graphene spin transport channel that is encapsulated between the top and bottom-hBN dielectrics, by considering the uncertainties in τ_s. Figure (**a**) is reproduced with permission from Ref. [3], ©2012 American Physical Society; (**b**) from Ref. [75], ©2015 American Chemical Society.

spin relaxation mechanisms, indicating that neither of these mechanisms dominate the spin relaxation in graphene on hBN in the presence of polymer residues.

To investigate the spin relaxation in the absence of polymer residues, a new device geometry[device B3 in Fig. 8.2] was employed to study spin transport, wherein a bilayer-graphene flake is encapsulated between a hBN substrate and a pre-patterned hBN strip [76] consisting of tunnel contacts with MgO barriers. Even though their results indicate the presence of resonant scattering spin relaxation mechanism [153], there has been no general consensus on the exact nature of spin relaxation mechanism in bilayer-graphene. In this architecture, polymers can still come in contact with graphene at the open areas of the pre-patterned hBN strip. In order to further reduce the size of the graphene regions exposed to polymer residues, a full encapsulation geometry [71, 72] [device A3 in Fig. 8.2] is adopted.

Even though the top-layer of a thin(1-2L) hBN tunnel barrier in a fully hBN encapsulated graphene spin valve device [71, 72] acts as an encapsulation layer, the resulting charge and spin transport properties of graphene are not optimal. Despite finding a suitable device geometry[device A3 in Fig. 8.2] to enhance the differential spin injection efficiency up to 100% in a fully hBN encapsulated graphene, the spin lifetime obtained only up to 0.9-1.86 ns with bilayer hBN tunnel barriers [70, 72]

[Fig. 8.4], are still smaller by two orders of magnitude than the predicted value for pristine graphene [1, 2]. An interesting study of spin relaxation in graphene with mono and bilayer of hBN encapsulating tunnel barrier is reported by Singh *et al*. [70]. The authors report τ_s above 1 ns for bilayer-hBN encapsulation while it is below 0.6 ns for the monolayer encapsulation. These observations indicate that a very thin ($\sim$ 0.3-0.7 nm) top-layer of single or bilayer-hBN tunnel barrier might not provide sufficient encapsulation for graphene, possibly due to poor screening of the polymer contaminations on the top-surface. Moreover, the screening effect is stronger with the bilayer than the monolayer-hBN. Also, the contact induced relaxation is expectedly lower with the bilayer-hBN barrier due to its higher R_cA product. In fact, these observations corroborate with the independent studies from Gurram *et al.* who reported τ_s around 0.3 ns, 0.9 ns, and 1.3 ns with mono [71], bi [72], and tri-layers [113] of hBN barrier top encapsulation, respectively [Fig. 8.4]. From these reports it seems that increasing the thickness of the top encapsulated tunnel barrier can enhance the screening of the contaminations and improve τ_s of the encapsulated graphene. However, the currently existing literature on fully hBN encapsulated graphene devices [71, 72] is limited and does not report the carrier density dependence of the spin relaxation time which is necessary for investigating the spin relaxation mechanism [3, 76]. Therefore, there is a need for more experiments to confirm the hBN barrier thickness dependence on spin transport in graphene and elucidate the intrinsic spin relaxation mechanism in graphene.

8.8 Future perspectives and conclusions

In order to reach the ultimate goals of spintronics devices [12, 13], several recently emerged spintronics phenomena need to be understood and incorporated in future graphene spin transport studies. In the following, we describe a few prospects which can be utilized in graphene-hBN heterostructures to facilitate the progress of graphene spintronics in the near future.

8.8.1 Device geometries

A possible solution to reduce the influence of the residues on top-surface of the thin (1-3 layer) hBN tunnel barrier on the spin relaxation in graphene[device A3 in Fig. 8.2] is to use the following three device geometeries for probing the spin transport in graphene: i) device B4 in Fig. 8.2 where a pre-patterned thick hBN layer on top of the hBN tunnel barrier acts as a protection layer from the lithographic residuals, except for the electrode deposition regions, ii) device A4 in Fig. 8.2 with 1D FM edge contacts which completely keeps the residues away from graphene by fully encapsulating with thick hBN layers. The recent reports [73, 107] showed the possibility of spin injection

through 1D FM contacts and these contacts are yet to be proven viable for efficient spin injection and detection. iii)even though bottom up fabricated devices with MgO barriers[device C3 in Fig. 8.2] showed the highest reported τ_s and λ_s by avoiding polymer contamination, the oxide barriers might still be influencing the spin transport in graphene. Therefore, the transfer of hBN-barrier/graphene/thick-large-hBN stacks onto pre-deposited FM electrodes[device C4 in Fig. 8.2] could avoid problems with oxide barriers and polymers altogether.

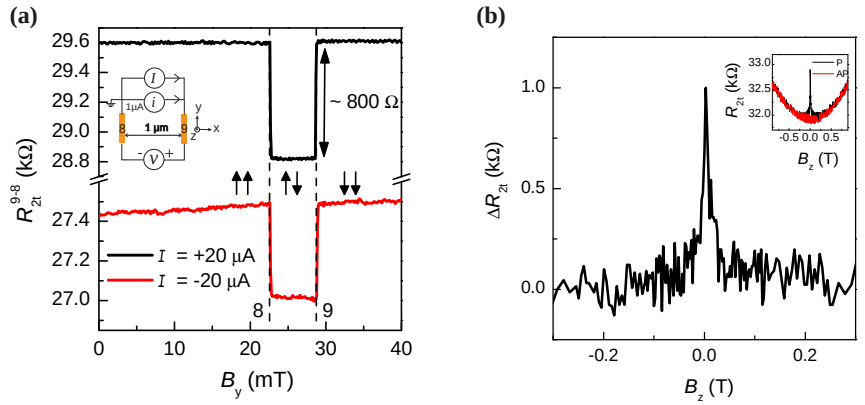

Figure 8.8: Large two-terminal spin valve and two-terminal Hanle spin precession signals in a fully hBN encapsulated graphene with bilayer-hBN tunnel barrier. (**a**) Large inverted two-terminal differential resistance $R_{2t} = v/i$, measured in a spin valve measurement configuration, at two different DC current bias I values, as a function of the magnetic field B_y applied along the easy-axes of the ferromagnetic cobalt electrodes. Inversion of the two-terminal spin valve signal is due to the two contacts biased with opposite polarity. The inset shows a schematic of the two-terminal spin valve measurement geometry. Vertical dashed lines represent the magnetization switching fields of the two contacts. (**b**) Two-terminal Hanle spin signal $\Delta R_{2t} = R_{2t}^{P} - R_{2t}^{AP}$ measured at DC current bias I = +20 μA, as a function of the magnetic field B_z applied perpendicular to the plane of spin injection. The inset shows the two-terminal differential resistance $R_{2t}^{P(AP)}$ measured as a function of B_z when the relative orientation of the magnetization of the contacts is aligned in parallel (P) and anti-parallel (AP) configurations. Figure (**a**) is reproduced with permission from Ref. [72], ©2017 Nature Publishing Group; (**b**) from Ref. [113].

8.8.2 Spin filtering across hBN/graphene interfaces

Spin filtering is technologically attractive as it gives efficient spin injection with only one type of spin polarized carrier transport. Spin filtering across a 2D material was first theoretically proposed by Karpan *et al.* [154, 155], who predicted that graphene

or graphite on lattice matched surfaces of nickel or cobalt behaves like a half-metal and can be used to inject a 100% spin polarized current in to nonmagnetic conductors. Rather low values of magnetoresistance were found experimentally due to disorder at the FM/graphene interface [156–159]. Thereafter, it was predicted that due to almost matched in-plane lattice constants of graphene and hBN, a FM/fewlayer-graphene/hBN junction can act as an ideal spin filter with an increased R_cA product [160–162], which is essential for avoiding the conductivity mismatch problem for efficient spin injection in graphene [163]. Along this direction, first principles calculations by Wu *et al.* [148] predicted that a FM/hBN/graphene junction allows only one type of spin to tunnel and results in an increase of injection current spin polarization up to 100% with the increase in the number of hBN layers up to three layers.

Recent experimental results on lateral spin valve devices with thick (2-3 layers) and highly resistive CVD-hBN tunnel barriers [69] showed a very large and inverted spin polarization in graphene which was attributed to the spin-filtering processes across the Co/thick-layer-CVD-hBN/graphene tunnel contacts. On the other hand, the results with Co/exfoliated-bilayer-hBN/graphene tunnel contacts [72] showed an enhanced differential spin injection/detection polarizations up to 100% as a function of bias and a sign reversal of the polarization close to zero bias. These results indicate that the graphene/hBN heterostructures provide a platform to explore the possibility of spin filtering in depth.

8.8.3 Spin gating

Electrical manipulation of the charge current in graphene is possible via electrostatic (charge) gating, for example, in field-effect transistors [14, 88], single-electron tunneling transistors [164, 165], and quantum dots [166]. A similar analogy can be applied for the manipulation of the spin accumulation in graphene, due to spin-orbit coupling (SOC), via "spin gating" [167].

Pristine graphene is non-magnetic [168] and has a small SOC [123] which makes it difficult for having an electrical control over the spins in graphene. One mechanism for achieving spin gating in graphene is via the Rashba spin-orbit field which can be created by the application of top and bottom gate voltages in a hBN/graphene/hBN heterostructure, as reported by Guimarães *et al.* [74][device B2 in Fig. 8.2]. The modulation of the spin-orbit coupling strength created in the hBN encapsulated part of graphene can be used for manipulating the spin polarized currents and thereby achieving the spin gating phenomenon. Essentially, one can realize a spintronic logic device like Datta Das spin transistor [169] with graphene by achieving its three important operating principles [170]: i)efficient and bias controlled spin injection and ii)detection [69, 72], and iii)spin manipulation via spin gating [74].

8.8.4 Spin drift

Spin transport in graphene has been widely studied in terms of diffusion of the spin accumulation. In general, the diffusion process equally distributes the spin accumulation in every direction, allowing only a fraction of the injected spins reaching the detector located away from the injector. Spin transport experiments in graphene have been performed in narrow (typical width $\sim$ 1-5 µm) transport channels, and analysed by assuming a uniform spin injection along the width of graphene flake and thus restricting the spin diffusion to one dimension along the length of the graphene. Even then, the spin accumulation diffuses in either side of the injector, resulting in only 50% of the injected spin directed towards the detector.

Due to the diffusive motion, the spin information is not directional and transported over only limited distances. On the other hand, when an electric field is applied across the spin transport channel, the electron spins acquire an additional drift velocity which is unidirectional along(opposite to) the electric field $\vec{E}$ for holes(electrons), and allows for a long distance spin transport.Note that the drift velocity $\vec{v}$ is proportional to the mobility μ of carriers, $\vec{v} = \mu\vec{E}$. Since the graphene encapsulated between top and bottom thick-hBN dielectrics has been reported to show high mobility [87, 99], the heterostructures of graphene-hBN are attractive for spin drift experiments. The first experimental proof of spin drift in graphene was provided by Józsa *et al*. [52], whose results were constrained by the lower mobility of graphene on SiO_2 substrate [device A1 in Fig. 8.2]. Recent spin drift experiments reported by Ingla-Ayńes *et al*. [75] using a thick-hBN encapsulated high-mobility bilayer-graphene spin transport channel [device B2 in Fig. 8.2] resulted in a strong modulation of the spin relaxation length up to 90 µm, and an effective steering of the spin accumulation with up to 88% efficiency[Fig. 8.7(b)], which is predicted to reach 100% in a fully hBN encapsulated graphene. Such an efficient control over directionality of spin current and long distance spin transport is enabled by the high-mobility of hBN encapsulated graphene devices. Moreover, considering a device geometry [e.g., B4 in Fig. 8.2], which combines high mobility graphene [e.g., device A2 in Fig. 8.2] with a large spin injection/detection polarized contacts [e.g., device A3 in Fig. 8.2] is highly attractive for applications in more complex spin based logic devices.

8.8.5 Proximity effects

Recent theoretical studies [151, 152] shed light on the potential of inducing magnetic exchange interactions via the electrostatic gating in cobalt/(1-4 layer)hBN/graphene heterostructures. First-principle already calculations [152] showed that by tuning the external electric field, the sign of the proximity induced equilibrium spin polarization in graphene can be reversed. It was also predicted [151] that even a very thin layer of hBN can be used as a gate dielectric, and by tuning the gate electric field in

a cobalt/hBN/graphene structure, both the sign and magnitude of the induced magnetization in graphene can be changed. These two studies are relevant to the hBN tunnel barrier encapsulated graphene spin valve device geometry[devices A3, B4 and C4 in Fig. 8.2] reported in the recent study [72]. In principle, the exchange interaction in graphene should also reflect in a modified shape of the Hanle spin precession signal [34]. Therefore, further investigation is needed to understand these results and also to elucidate the effect of the sign of the charge carriers, i.e., electrons or holes. Interestingly, recent experimental studies [107, 171] revealed the possibility of inducing spin splitting states in graphene by bringing in proximity to a ferromagnet.

8.8.6 Large-scale devices

The growth of spintronic materials using the CVD process is a promising route for industry-scale spintronic applications. However, due to the challenges involved in the impurity-free transfer and device fabrication, there are only few reports on spin transport studies with CVD grown graphene and hBN. Spin valve devices prepared with CVD graphene transferred on to SiO_2/Si substrate showed limited spin transport characteristics [63, 68, 134, 172–174] with τ_s below 1.2 ns and λ_s below 6 µm at room temperature. Such low performance compared to exfoliated flakes is caused by the wet transfer process used for transferring the CVD graphene. So far, the longest spin lifetime of 1.75 ns is achieved for CVD graphene [78] in inverted spin valve devices prepared by the dry-transfer technique [175]. Initial efforts on integration of large scale CVD grown hBN as a tunnel barrier for graphene spin valve devices successfully demonstrated the spin injection and detection [67, 68]. The recently reported large magnitude of spin injection polarization up to 65% at bias above 1.5 V using contacts with thick(1-3L)-layer-CVD-hBN tunnel barriers [69], and up to 15% at -0.2 V bias using two-layer-stacked-CVD-hBN barriers [8] indicates the promising nature of CVD-hBN for large-scale spintronics applications.

However, in order to establish the role of CVD based graphene and hBN in spintronics, it is important to prepare high quality graphene-hBN heterostructures. For this, a controlled growth of CVD-hBN [176] followed by its dry transfer on top of a recently obtained high-quality CVD-graphene [175] could help to progress the role of CVD grown materials [8] for practical spintronics devices. Moreover, a direct growth of hBN on graphene would solve the quality problems [8] associated with the conventional polymer based wet transfer method [177].

8.8.7 Conclusions

A decade since the first reported non-local spin transport and spin precession in graphene field-effect transistor [15], the spintronics research has been focusing on improving the spin transport parameters viz., achieving large spin relaxation time by bottom-up

hBN/graphene structures [5, 77], long spin relaxation length by the spin drift effect in the hBN encapsulated graphene [75], and an efficient spin injection/detection polarization up to 100% by external bias across cobalt/2L-hBN/graphene contacts [72]. Besides, there is still a need to clarify the debate about which of the EY, DP, and resonant scattering mechanisms causes spin relaxation in graphene [149, 178]. Since the influence of surroundings is minimal in a fully hBN encapsulated graphene heterostructure, it provides a perfect platform to demystify the intrinsic spin relaxation mechanism in graphene [5, 62, 63].

Furthermore, the sensitivity of graphene can be exploited in studying the proximity effects by integrating with other 2D materials. The recent emergence of number of publications in the literature on the proximity studies speaks for its importance. Magnetic proximity effects can be studied in graphene in proximity with 2D ferromagnetic materials such as CrI_3 [179], $Cr_2Ge_2Te_6$, [180] and $MnSe_2$ [181]. In future, it would be interesting to demonstrate a graphene spin valve heterostructure completely made out of 2D materials. For example, CrI_3/(1-3L)hBN/graphene/thick-hBN where CrI_3 acts as a 2D ferromagnetic source for inducing spin accumulation in graphene, 1-3L hBN acts as a 2D tunnel barrier, and thick-hBN acts as a bottom substrate. Besides, the proximity of a TMDC to induce spin-orbit coupling in graphene will add new functionalities to spintronic devices [36–47].

In conclusion, graphene-hBN heterostructures have been the stepping stone in revolutionizing and redefining the research of spin transport in graphene, enabling an order of magnitude improvement in the spin-injection/detection and transport parameters. The obtained results are quite promising, and with the available technology and understanding, and by adapting new device geometries proposed in this review, the figure of merit of the graphene spintronic devices can be improved further.

8.9 Acknowledgements

This project has received funding from the European Union Horizon 2020 research and innovation programme under grant agreement No. 696656, supported by the Zernike Institute for Advanced Materials and is (partly) financed by the NWO Spinoza prize awarded to Prof. B.J. van Wees by the Nederlandse Organisatie voor Wetenschappelijk Onderzoek (NWO). We would also like to thank Dr. M. Venkata Kamalakar, Prof. B Beschoten, and Ingla-Aynés for providing the original figures.

References

[1] Huertas-Hernando, D., Guinea, F. & Brataas, A. Spin-orbit coupling in curved graphene, fullerenes, nanotubes, and nanotube caps. *Phys. Rev. B* **74**, 155426 (2006).

[2] Kane, C. L. & Mele, E. J. Quantum Spin Hall effect in graphene. *Phys. Rev. Lett.* **95**, 226801 (2005).

[3] Zomer, P. J. *et al.* Long-distance spin transport in high-mobility graphene on hexagonal boron nitride. *Phys. Rev. B* **86**, 161416 (2012).

[4] Ingla-Aynés, J. *et al.* 24 μm spin relaxation length in boron nitride encapsulated bilayer graphene. *Phys. Rev. B* **92**, 201410 (2015).

[5] Drögeler, M. *et al.* Spin lifetimes exceeding 12 ns in graphene nonlocal spin valve devices. *Nano Lett.* **16**, 3533–3539 (2016).

[6] Han, W. & Kawakami, R. K. Spin relaxation in single-layer and bilayer graphene. *Phys. Rev. Lett.* **107**, 047207 (2011).

[7] Józsa, C. *et al.* Linear scaling between momentum and spin scattering in graphene. *Phys. Rev. B* **80**, 241403 (2009).

[8] Gurram, M. *et al.* Spin transport in two-layer-CVD-hBN/graphene/hBN heterostructures. *Phys. Rev. B* **97**, 045411 (2018).

[9] Elliott, R. J. Theory of the effect of spin-orbit coupling on magnetic resonance in some semiconductors. *Phys. Rev.* **96**, 266–279 (1954).

[10] Yafet, Y. g factors and spin-lattice relaxation of conduction electrons. *Solid state physics* **14**, 1–98 (1963).

[11] D'yakonov, M. & Perel, V. Spin orientation of electrons associated with the interband absorption of light in semiconductors. *Soviet Journal of Experimental and Theoretical Physics* **33**, 1053 (1971).

[12] Han, W. *et al.* Graphene spintronics. *Nature Nano.* **9**, 794–807 (2014).

[13] Roche, S. *et al.* Graphene spintronics: The European Flagship perspective. *2D Mater.* **2**, 030202 (2015).

[14] Novoselov, K. S. *et al.* Electric field effect in atomically thin carbon films. *Science* **306**, 666–669 (2004).

[15] Tombros, N. *et al.* Electronic spin transport and spin precession in single graphene layers at room temperature. *Nature* **448**, 571–574 (2007).

[16] Han, W. *et al.* Tunneling spin injection into single layer graphene. *Phys. Rev. Lett.* **105**, 167202 (2010).

[17] Tombros, N. *et al.* Anisotropic spin relaxation in graphene. *Phys. Rev. Lett.* **101**, 046601 (2008).

[18] Popinciuc, M. *et al.* Electronic spin transport in graphene field-effect transistors. *Phys. Rev. B* **80**, 214427 (2009).

[19] Yang, T.-Y. *et al.* Observation of long spin-relaxation times in bilayer graphene at room temperature. *Phys. Rev. Lett.* **107**, 047206 (2011).

[20] Maassen, T. *et al.* Comparison between charge and spin transport in few-layer graphene. *Phys. Rev. B* **83**, 115410 (2011).

[21] Sabio, J. *et al.* Electrostatic interactions between graphene layers and their environment. *Phys. Rev. B* **77**, 195409 (2008).

[22] Chen, J.-H. *et al.* Charged-impurity scattering in graphene. *Nature Phys.* **4**, 377–381 (2008).

[23] Ertler, C. *et al.* Electron spin relaxation in graphene: The role of the substrate. *Phys. Rev. B* **80**, 041405 (2009).

[24] Tuan, D. V. *et al.* Spin dynamics and relaxation in graphene dictated by electron-hole puddles. *Sci. Rep.* **6**, 21046 (2016).

[25] Martin, J. *et al.* Observation of electronhole puddles in graphene using a scanning single-electron transistor. *Nature Phys.* **4**, 144–148 (2008).

[26] Du, X. *et al.* Approaching ballistic transport in suspended graphene. *Nature Nano.* **3**, 491–495 (2008).

[27] Bao, W. *et al.* Controlled ripple texturing of suspended graphene and ultrathin graphite membranes. *Nature Nano.* **4**, 562–566 (2009).

[28] Guimarães, M. H. D. *et al.* Spin transport in high-quality suspended graphene devices. *Nano Lett.* **12**, 3512–3517 (2012).

[29] Neumann, I. *et al.* Electrical detection of spin precession in freely suspended graphene spin valves on cross-linked poly(methyl methacrylate). *Small* **9**, 156–160 (2013).

[30] Maassen, T. *et al.* Long spin relaxation times in wafer scale epitaxial graphene on SiC0001. *Nano Lett.* **12**, 1498–1502 (2012).

[31] Dlubak, B. *et al.* Highly efficient spin transport in epitaxial graphene on SiC. *Nature Phys.* **8**, 557–561 (2012).
[32] Maassen, T. *et al.* Localized states influence spin transport in epitaxial graphene. *Phys. Rev. Lett.* **110**, 067209 (2013).
[33] Yan, W. *et al.* Long spin diffusion length in few-layer graphene flakes. *Phys. Rev. Lett.* **117**, 147201 (2016).
[34] Leutenantsmeyer, J. C. *et al.* Proximity induced room temperature ferromagnetism in graphene probed with spin currents. *2D Mater.* **4**, 014001 (2017).
[35] Singh, S. *et al.* Strong modulation of spin currents in bilayer graphene by static and fluctuating proximity exchange fields. *Phys. Rev. Lett.* **118**, 187201 (2017).
[36] Cummings, A. W. *et al.* Giant spin lifetime anisotropy in graphene induced by proximity effects. *Phys. Rev. Lett.* **119**, 206601 (2017).
[37] Garcia, J. H., Cummings, A. W. & Roche, S. Spin hall effect and weak antilocalization in graphene/transition metal dichalcogenide heterostructures. *Nano Lett.* **17**, 5078–5083 (2017).
[38] Gmitra, M. *et al.* Trivial and inverted dirac bands and the emergence of quantum spin hall states in graphene on transition-metal dichalcogenides. *Phys. Rev. B* **93**, 155104 (2016).
[39] Yan, W. *et al.* A two-dimensional spin field-effect switch. *Nat. Commun.* **7**, 13372 (2016).
[40] Wang, Z. *et al.* Strong interface-induced spinorbit interaction in graphene on WS_2. *Nat. Commun.* **6**, 8339 (2015).
[41] Omar, S. & van Wees, B. J. Graphene-WS_2 heterostructures for tunable spin injection and spin transport. *Phys. Rev. B* **95**, 081404 (2017).
[42] Omar, S. & van Wees, B. J. Spin transport in high-mobility graphene on WS_2 substrate with electric-field tunable proximity spin-orbit interaction. *Phys. Rev. B* **97**, 045414 (2018).
[43] Dankert, A. & Dash, S. P. Electrical gate control of spin current in van der waals heterostructures at room temperature. *Nat. Commun.* **8**, 16093 (2017).
[44] Luo, Y. K. *et al.* Opto-valleytronic spin injection in monolayer MoS_2/Few-layer graphene hybrid spin valves. *Nano lett.* **17**, 3877–3883 (2017).
[45] Avsar, A. *et al.* Optospintronics in graphene via proximity coupling. *ACS Nano* **11**, 11678–11686 (2017).
[46] Ghiasi, T. S. *et al.* Large proximity-induced spin lifetime anisotropy in transition-metal dichalcogenide/graphene heterostructures. *Nano lett.* **17**, 7528–7532 (2017).
[47] Benitez, L. *et al.* Strongly anisotropic spin relaxation in graphene/WS_2 van der waals heterostructures. *arXiv:1710.11568* (2017).
[48] Hill, E. W. *et al.* Graphene spin valve devices. *IEEE Transactions on Magnetics* **42**, 2694–2696 (2006).
[49] Nishioka, M. & Goldman, A. M. Spin transport through multilayer graphene. *Appl. Phys. Lett.* **90**, 252505 (2007).
[50] Ohishi, M. *et al.* Spin injection into a graphene thin film at room temperature. *Jpn. J. Appl. Phys.* **46**, L605 (2007).
[51] Cho, S., Chen, Y.-F. & Fuhrer, M. S. Gate-tunable graphene spin valve. *Appl. Phys. Lett.* **91**, 123105 (2007).
[52] Józsa, C. *et al.* Electronic spin drift in graphene field-effect transistors. *Phys. Rev. Lett.* **100**, 236603 (2008).
[53] Wang, W. H. *et al.* Growth of atomically smooth MgO films on graphene by molecular beam epitaxy. *Appl. Phys. Lett.* **93**, 183107 (2008).
[54] Han, W. *et al.* Electron-hole asymmetry of spin injection and transport in single-layer graphene. *Phys. Rev. Lett.* **102**, 137205 (2009).
[55] Józsa, C. *et al.* Controlling the efficiency of spin injection into graphene by carrier drift. *Phys. Rev. B* **79**, 081402 (2009).
[56] Dlubak, B. *et al.* Are Al_2O_3 and MgO tunnel barriers suitable for spin injection in graphene? *Appl.*

Phys. Lett. **97**, 092502 (2010).

[57] Han, W. *et al.* Spin relaxation in single-layer graphene with tunable mobility. *Nano Lett.* **12**, 3443–3447 (2012).

[58] Yamaguchi, T. *et al.* Tunnel spin injection into graphene using Al_2O_3 barrier grown by atomic layer deposition on functionalized graphene surface. *J. Magn. Magn. Mater.* **324**, 849–852 (2012).

[59] Volmer, F. *et al.* Role of MgO barriers for spin and charge transport in Co/MgO/graphene nonlocal spin-valve devices. *Phys. Rev. B* **88**, 161405 (2013).

[60] Omar, S. *et al.* Spin relaxation in graphene with self-assembled cobalt porphyrin molecules. *Phys. Rev. B* **92**, 115442 (2015).

[61] Canto, B. *et al.* On the structural and chemical characteristics of Co/Al_2O_3/graphene interfaces for graphene spintronic devices. *Sci. Rep.* **5**, 14332 (2015).

[62] Amamou, W. *et al.* Contact induced spin relaxation in graphene spin valves with Al_2O_3 and MgO tunnel barriers. *APL Mater.* **4**, 032503 (2016).

[63] Stecklein, G. *et al.* Contact-induced spin relaxation in graphene nonlocal spin valves. *Phys. Rev. Appl.* **6**, 054015 (2016).

[64] Wen, H. *et al.* Experimental demonstration of XOR operation in graphene magnetologic gates at room temperature. *Phys. Rev. Appl.* **5**, 044003 (2016).

[65] Yamaguchi, T. *et al.* Electrical spin injection into graphene through monolayer hexagonal boron nitride. *Appl. Phys. Express* **6**, 073001 (2013).

[66] Kamalakar, M. V. *et al.* Enhanced tunnel spin injection into graphene using chemical vapor deposited hexagonal boron nitride. *Sci. Rep.* **4**, 6146 (2014).

[67] Kamalakar, M. V. *et al.* Spintronics with graphene-hexagonal boron nitride van der Waals heterostructures. *Appl. Phys. Lett.* **105**, 212405 (2014).

[68] Fu, W. *et al.* Large-scale fabrication of BN tunnel barriers for graphene spintronics. *J. Appl. Phys.* **116**, 074306 (2014).

[69] Kamalakar, M. V. *et al.* Inversion of spin signal and spin filtering in ferromagnet—hexagonal boron nitride-graphene van der Waals heterostructures. *Sci. Rep.* **6**, 21168 (2016).

[70] Singh, S. *et al.* Nanosecond spin relaxation times in single layer graphene spin valves with hexagonal boron nitride tunnel barriers. *Appl. Phys. Lett.* **109**, 122411 (2016).

[71] Gurram, M. *et al.* Spin transport in fully hexagonal boron nitride encapsulated graphene. *Phys. Rev. B* **93**, 115441 (2016).

[72] Gurram, M., Omar, S. & van Wees, B. J. Bias induced up to 100% spin-injection and detection polarizations in ferromagnet/bilayer-hBN/graphene/hBN heterostructures. *Nat. Commun.* **8**, 248 (2017).

[73] Karpiak, B. *et al.* 1D ferromagnetic edge contacts to 2D graphene/h-BN heterostructures. *2D Mater.* **5**, 014001 (2017).

[74] Guimarães, M. H. D. *et al.* Controlling spin relaxation in hexagonal BN-encapsulated graphene with a transverse electric field. *Phys. Rev. Lett.* **113**, 086602 (2014).

[75] Ingla-Aynés, J., Meijerink, R. J. & van Wees, B. J. Eighty-eight percent directional guiding of spin currents with 90 μm relaxation length in bilayer graphene using carrier drift. *Nano Lett.* **16**, 4825–4830 (2016).

[76] Avsar, A. *et al.* Electronic spin transport in dual-gated bilayer graphene. *NPG Asia Mater.* **8**, e274 (2016).

[77] Drögeler, M. *et al.* Nanosecond spin lifetimes in single- and few-layer graphene-hBN heterostructures at room temperature. *Nano Lett.* **14**, 6050–6055 (2014).

[78] Drögeler, M. *et al.* Dry-transferred cvd graphene for inverted spin valve devices. *Appl. Phys. Lett.* **111**, 152402 (2017).

[79] Giovannetti, G. *et al.* Substrate-induced band gap in graphene on hexagonal boron nitride: Ab initio density functional calculations. *Phys. Rev. B* **76**, 073103 (2007).

[80] Watanabe, K., Taniguchi, T. & Kanda, H. Direct-bandgap properties and evidence for ultraviolet lasing of hexagonal boron nitride single crystal. *Nat. Mater.* **3**, 404–409 (2004).

[81] Novoselov, K. S. *et al.* Two-dimensional atomic crystals. *Proceedings of the National Academy of Sciences of the United States of America* **102**, 10451–10453 (2005).

[82] Gorbachev, R. V. *et al.* Hunting for monolayer boron nitride: Optical and Raman signatures. *Small* **7**, 465–468 (2011).

[83] Xue, J. *et al.* Scanning tunnelling microscopy and spectroscopy of ultra-flat graphene on hexagonal boron nitride. *Nat. Mater.* **10**, 282–285 (2011).

[84] Neumann, C. *et al.* Raman spectroscopy as probe of nanometre-scale strain variations in graphene. *Nat. Commun.* **6**, 8429 (2015).

[85] Young, A. F. *et al.* Electronic compressibility of layer-polarized bilayer graphene. *Phys. Rev. B* **85**, 235458 (2012).

[86] Hattori, Y. *et al.* Layer-by-layer dielectric breakdown of hexagonal boron nitride. *ACS Nano* **9**, 916–921 (2015).

[87] Dean, C. R. *et al.* Boron nitride substrates for high-quality graphene electronics. *Nature Nano.* **5**, 722–726 (2010).

[88] Britnell, L. *et al.* Field-effect tunneling transistor based on vertical graphene heterostructures. *Science* **335**, 947–950 (2012).

[89] Ponomarenko, L. A. *et al.* Effect of a high-κ environment on charge carrier mobility in graphene. *Phys. Rev. Lett.* **102**, 206603 (2009).

[90] Amet, F. *et al.* Tunneling spectroscopy of graphene-boron-nitride heterostructures. *Phys. Rev. B* **85**, 073405 (2012).

[91] Zomer, P. *et al.* A transfer technique for high mobility graphene devices on commercially available hexagonal boron nitride. *Appl. Phys. Lett.* **99**, 232104 (2011).

[92] Azizi, A. *et al.* Freestanding van der waals heterostructures of graphene and transition metal dichalcogenides. *ACS nano* **9**, 4882–4890 (2015).

[93] Han, G. H. *et al.* Continuous growth of hexagonal graphene and boron nitride in-plane heterostructures by atmospheric pressure chemical vapor deposition. *ACS Nano* **7**, 10129–10138 (2013).

[94] Fu, L. *et al.* Direct growth of MoS_2/h-BN heterostructures via a sulfide-resistant alloy. *ACS Nano* **10**, 2063–2070 (2016).

[95] Mishra, N. *et al.* Rapid and catalyst-free van der waals epitaxy of graphene on hexagonal boron nitride. *Carbon* **96**, 497–502 (2016).

[96] Reina, A. *et al.* Transferring and identification of single- and few-layer graphene on arbitrary substrates. *The Journal of Physical Chemistry C* **112**, 17741–17744 (2008).

[97] Dean, C. R. *et al.* Multicomponent fractional quantum Hall effect in graphene. *Nature Phys.* **7**, 693–696 (2011).

[98] Garcia, A. G. F. *et al.* Effective cleaning of hexagonal boron nitride for graphene devices. *Nano Lett.* **12**, 4449–4454 (2012).

[99] Mayorov, A. S. *et al.* Micrometer-scale ballistic transport in encapsulated graphene at room temperature. *Nano Lett.* **11**, 2396–2399 (2011).

[100] Ishigami, M. *et al.* Atomic structure of graphene on SiO_2. *Nano Lett.* **7**, 1643–1648 (2007).

[101] Haigh, S. J. *et al.* Cross-sectional imaging of individual layers and buried interfaces of graphene-based heterostructures and superlattices. *Nat. Mater.* **11**, 764–767 (2012).

[102] Lindvall, N., Kalabukhov, A. & Yurgens, A. Cleaning graphene using atomic force microscope. *J. Appl. Phys.* **111**, 064904 (2012).

[103] Leon, J. A. *et al.* Transferring few-layer graphene sheets on hexagonal boron nitride substrates for fabrication of graphene devices. *Graphene* **03**, 25 (2014).

[104] Yamaguchi, J. *et al.* Passivating chemical vapor deposited graphene with metal oxides for transfer and transistor fabrication processes. *Appl. Phys. Lett.* **102**, 143505 (2013).

[105] Robinson, J. A. *et al.* Contacting graphene. *Appl. Phys. Lett.* **98**, 053103 (2011).

[106] Wang, L. *et al.* One-dimensional electrical contact to a two-dimensional material. *Science* **342**, 614–617 (2013).

[107] Xu, J. *et al.* Spin inversion in graphene spin valves by gate-tunable magnetic proximity effect at one-dimensional contacts. *arXiv* **1802.07790** (2018).

[108] Zomer, P. J. *et al.* Fast pick up technique for high quality heterostructures of bilayer graphene and hexagonal boron nitride. *Appl. Phys. Lett.* **105**, 013101 (2014).

[109] Pizzocchero, F. *et al.* The hot pick-up technique for batch assembly of van der waals heterostructures. *Nat. Commun.* **7**, 11894 (2016).

[110] Castellanos-Gomez, A. *et al.* Deterministic transfer of two-dimensional materials by all-dry viscoelastic stamping. *2D Mater.* **1**, 011002 (2014).

[111] Uwanno, T. *et al.* Fully dry PMMA transfer of graphene on h -BN using a heating/cooling system. *2D Mater.* **2**, 041002 (2015).

[112] Yang, R. *et al.* Multilayer MoS_2 transistors enabled by a facile dry-transfer technique and thermal annealing. *Journal of Vacuum Science & Technology B, Nanotechnology and Microelectronics: Materials, Processing, Measurement, and Phenomena* **32**, 061203 (2014).

[113] Gurram, M., Omar, S. & van Wees, B. J. *Unpublished* .

[114] Castro Neto, A. H. & Guinea, F. Impurity-induced spin-orbit coupling in graphene. *Phys. Rev. Lett.* **103**, 026804 (2009).

[115] Goossens, A. M. *et al.* Mechanical cleaning of graphene. *Appl. Phys. Lett.* **100**, 073110 (2012).

[116] Yuasa, S. *et al.* Giant tunneling magnetoresistance up to 410% at room temperature in fully epitaxial CoMgOCo magnetic tunnel junctions with bcc Co(001) electrodes. *Appl. Phys. Lett.* **89**, 042505 (2006).

[117] Drögeler, M. *et al.* Nanosecond spin lifetimes in bottom-up fabricated bilayer graphene spin-valves with atomic layer deposited Al_2O_3 spin injection and detection barriers. *Phys. Status Solidi (B)* **252**, 2395–2400 (2015).

[118] Huang, Y. W. *et al.* Spin-valve transistor. *J. Appl. Phys.* **97**, 10D504 (2005).

[119] Filip, A. T. *et al.* Experimental search for the electrical spin injection in a semiconductor. *Phys. Rev. B* **62**, 9996–9999 (2000).

[120] Han, W. *et al.* Electrical detection of spin precession in single layer graphene spin valves with transparent contacts. *Appl. Phys. Lett.* **94**, 222109 (2009).

[121] Rashba, E. I. Theory of electrical spin injection: Tunnel contacts as a solution of the conductivity mismatch problem. *Phys. Rev. B* **62**, R16267–R16270 (2000).

[122] Fert, A. & Jaffrès, H. Conditions for efficient spin injection from a ferromagnetic metal into a semiconductor. *Phys. Rev. B* **64**, 184420 (2001).

[123] Min, H. *et al.* Intrinsic and Rashba spin-orbit interactions in graphene sheets. *Phys. Rev. B* **74**, 165310 (2006).

[124] Yao, Y. *et al.* Spin-orbit gap of graphene: First-principles calculations. *Phys. Rev. B* **75**, 041401 (2007).

[125] Maassen, T. *et al.* Contact-induced spin relaxation in hanle spin precession measurements. *Phys. Rev. B* **86**, 235408 (2012).

[126] Sosenko, E., Wei, H. & Aji, V. Effect of contacts on spin lifetime measurements in graphene. *Phys. Rev. B* **89**, 245436 (2014).

[127] Idzuchi, H., Fert, A. & Otani, Y. Revisiting the measurement of the spin relaxation time in graphene-based devices. *Phys. Rev. B* **91**, 241407 (2015).

[128] Dash, S. P. *et al.* Spin precession and inverted Hanle effect in a semiconductor near a finite-roughness ferromagnetic interface. *Phys. Rev. B* **84**, 054410 (2011).

[129] Garzon, S., Žutić, I. & Webb, R. A. Temperature-dependent asymmetry of the nonlocal spin-injection resistance: Evidence for spin nonconserving interface scattering. *Phys. Rev. Lett.* **94**, 176601 (2005).

[130] Park, J.-H. & Lee, H.-J. Out-of-plane magnetoresistance in ferromagnet/graphene/ferromagnet spin-valve junctions. *Phys. Rev. B* **89**, 165417 (2014).

[131] Li, B., Chen, L. & Pan, X. Spin-flip phenomena at the Co|graphene|Co interfaces. *Appl. Phys. Lett.* **98**, 133111 (2011).

[132] Volmer, F. *et al.* Suppression of contact-induced spin dephasing in graphene/MgO/Co spin-valve devices by successive oxygen treatments. *Phys. Rev. B* **90**, 165403 (2014).

[133] Wang, W. H. *et al.* Magnetotransport properties of mesoscopic graphite spin valves. *Phys. Rev. B* **77**, 020402 (2008).

[134] Avsar, A. *et al.* Toward wafer scale fabrication of graphene based spin valve devices. *Nano Lett.* **11**, 2363–2368 (2011).

[135] Abel, J. *et al.* Fabrication of an electrical spin transport device utilizing a diazonium salt/hafnium oxide interface layer on epitaxial graphene grown on 6 H-SiC (0001). *Journal of Vacuum Science & Technology B, Nanotechnology and Microelectronics: Materials, Processing, Measurement, and Phenomena* **30**, 04E109 (2012).

[136] Komatsu, K. *et al.* Spin injection and detection in a graphene lateral spin valve using an yttrium-oxide tunneling barrier. *Appl. Phys. Express* **7**, 085101 (2014).

[137] Singh, S. *et al.* Strontium oxide tunnel barriers for high quality spin transport and large spin accumulation in graphene. *Nano Lett.* (2017).

[138] Ahmed, A. S. *et al.* Molecular beam epitaxy growth of SrO buffer layers on graphite and graphene for the integration of complex oxides. *Journal of Crystal Growth* **447**, 5–12 (2016).

[139] Amamou, W. Spin and charge spin transport in 2d materials and magnetic insulator/metal heterostructures. *UC Riverside Electronic Theses and Dissertations* (2017).

[140] Friedman, A. L. *et al.* Hydrogenated graphene as a homoepitaxial tunnel barrier for spin and charge transport in graphene. *ACS Nano* **9**, 6747–6755 (2015).

[141] Friedman, A. L. *et al.* Homoepitaxial tunnel barriers with functionalized graphene-on-graphene for charge and spin transport. *Nat. Commun.* **5**, 3161 (2014).

[142] Neumann, I. *et al.* Enhanced spin accumulation at room temperature in graphene spin valves with amorphous carbon interfacial layers. *Appl. Phys. Lett.* **103**, 112401 (2013).

[143] Kamalakar, M. V., Dankert, A. & Dash, S. P. Spintronics with graphene and van der waals heterostructures. In *Contemporary Topics in Semiconductor Spintronics*, 241–258 (World Scientific, 2017).

[144] Lee, G.-H. *et al.* Electron tunneling through atomically flat and ultrathin hexagonal boron nitride. *Appl. Phys. Lett.* **99**, 243114 (2011).

[145] Britnell, L. *et al.* Electron tunneling through ultrathin boron nitride crystalline barriers. *Nano Lett.* **12**, 1707–1710 (2012).

[146] Jain, N. *et al.* Monolayer graphene/hexagonal boron nitride heterostructure. *Carbon* **54**, 396–402 (2013).

[147] Ji, Y. *et al.* Boron nitride as two dimensional dielectric: Reliability and dielectric breakdown. *Appl. Phys. Lett.* **108**, 012905 (2016).

[148] Wu, Q. *et al.* Efficient spin injection into graphene through a tunnel barrier: Overcoming the spin-conductance mismatch. *Phys. Rev. Appl.* **2**, 044008 (2014).

[149] Roche, S. & Valenzuela, S. O. Graphene spintronics: Puzzling controversies and challenges for spin manipulation. *J. Phys. D: Appl. Phys.* **47**, 094011 (2014).

[150] Allain, A. *et al.* Electrical contacts to two-dimensional semiconductors. *Nat. Mater.* **14**, 1195 (2015).

[151] Lazić, P., Belashchenko, K. D. & Žutić, I. Effective gating and tunable magnetic proximity effects in two-dimensional heterostructures. *Phys. Rev. B* **93**, 241401 (2016).

[152] Zollner, K. *et al.* Theory of proximity-induced exchange coupling in graphene on hBN/(Co, Ni). *Phys. Rev. B* **94**, 155441 (2016).

[153] Kochan, D. *et al.* Resonant Scattering by Magnetic Impurities as a Model for Spin Relaxation in Bilayer Graphene. *Phys. Rev. Lett.* **115**, 196601 (2015).

[154] Karpan, V. M. *et al.* Graphite and graphene as perfect spin filters. *Phys. Rev. Lett.* **99**, 176602 (2007).

[155] Karpan, V. M. *et al.* Theoretical prediction of perfect spin filtering at interfaces between close-packed

surfaces of Ni or Co and graphite or graphene. *Phys. Rev. B* **78**, 195419 (2008).

[156] Dlubak, B. *et al.* Graphene-passivated nickel as an oxidation-resistant electrode for spintronics. *ACS Nano* **6**, 10930–10934 (2012).

[157] Singh, A. K. & Eom, J. Negative magnetoresistance in a vertical single-layer graphene spin valve at room temperature. *ACS Applied Materials & Interfaces* **6**, 2493–2496 (2014).

[158] Godel, F. *et al.* Voltage-controlled inversion of tunnel magnetoresistance in epitaxial nickel/graphene/MgO/cobalt junctions. *Appl. Phys. Lett.* **105**, 152407 (2014).

[159] Cobas, E. D. *et al.* Room-temperature spin filtering in metallic ferromagnetmultilayer graphene-ferromagnet junctions. *ACS Nano* **10**, 10357–10365 (2016).

[160] Karpan, V. M. *et al.* Ni(111)|graphene|h-BN junctions as ideal spin injectors. *Phys. Rev. B* **84**, 153406 (2011).

[161] Yazyev, O. V. & Pasquarello, A. Magnetoresistive junctions based on epitaxial graphene and hexagonal boron nitride. *Phys. Rev. B* **80**, 035408 (2009).

[162] Hu, M. L. *et al.* Tunneling magnetoresistance of bilayer hexagonal boron nitride and its linear response to external uniaxial strain. *The Journal of Physical Chemistry C* **115**, 8260–8264 (2011).

[163] Schmidt, G. *et al.* Fundamental obstacle for electrical spin injection from a ferromagnetic metal into a diffusive semiconductor. *Phys. Rev. B* **62**, R4790–R4793 (2000).

[164] Stampfer, C. *et al.* Tunable graphene single electron transistor. *Nano Lett.* **8**, 2378 (2008).

[165] Epping, A. *et al.* Etched graphene single electron transistors on hexagonal boron nitride in high magnetic fields. *Phys. Status Solidi (b)* **250**, 2692–2696 (2013).

[166] Engels, S. *et al.* Etched graphene quantum dots on hexagonal boron nitride. *Appl. Phy. Lett.* **103**, 073113 (2013).

[167] Shekhter, R. & Jonson, M. Spin gating of mesoscopic devices. *Synthetic Metals* **216**, 2–10 (2016).

[168] Novoselov, K. S. *et al.* 2D materials and van der Waals heterostructures. *Science* **353** (2016).

[169] Datta, S. & Das, B. Electronic analog of the electro-optic modulator. *Appl. Phys. Lett.* **56**, 665–667 (1990).

[170] Semenov, Y. G., Kim, K. W. & Zavada, J. M. Spin field effect transistor with a graphene channel. *Appl. Phys. Lett.* **91**, 153105 (2007).

[171] Asshoff, P. *et al.* Magnetoresistance of vertical Co-graphene-NiFe junctions controlled by charge transfer and proximity-induced spin splitting in graphene. *2D Mater.* (2017).

[172] Wojtaszek, M. *et al.* Absence of hyperfine effects in ^{13}C-graphene spin-valve devices. *Phys. Rev. B* **89**, 035417 (2014).

[173] Kamalakar, M. V. *et al.* Long distance spin communication in chemical vapour deposited graphene. *Nat. Commun.* **6**, 6766 (2015).

[174] Anugrah, Y. *et al.* Independent gate control of injected and detected spin currents in CVD graphene nonlocal spin valves. *AIP Advances* **8**, 015129 (2018).

[175] Banszerus, L. *et al.* Ultrahigh-mobility graphene devices from chemical vapor deposition on reusable copper. *Sci. Adv.* **1**, e1500222 (2015).

[176] Gao, Y. *et al.* Repeated and controlled growth of monolayer, bilayer and few-layer hexagonal boron nitride on Pt foils. *ACS nano* **7**, 5199–5206 (2013).

[177] Lee, Y. *et al.* Wafer-scale synthesis and transfer of graphene films. *Nano Lett.* **10**, 490–493 (2010).

[178] Huertas-Hernando, D., Guinea, F. & Brataas, A. Spin-orbit-mediated spin relaxation in graphene. *Phys. Rev. Lett.* **103**, 146801 (2009).

[179] Huang, B. *et al.* Layer-dependent ferromagnetism in a van der Waals crystal down to the monolayer limit. *Nature* **546**, 270–273 (2017).

[180] Gong, C. *et al.* Discovery of intrinsic ferromagnetism in two-dimensional van der Waals crystals. *Nature* **546**, 265–269 (2017).

[181] Kan, M., Adhikari, S. & Sun, Q. Ferromagnetism in MnX_2 (X = S, Se) monolayers. *Physical Chemistry Chemical Physics* **16**, 4990–4994 (2014).